THESIS FOR DEGREE OF LICENTIATE OF ENGINEERING

Powder degradation during powder bed fusion processing

AHMAD RAZA

Department of Industrial and Materials Science

CHALMERS UNIVERSITY OF

TECHNOLOGY Gothenburg, Sweden, 2021

POWDER DEGRADATION DURING POWDER BED FUSION PROCESSING

Ahmad Raza

No. IMS-2021-18

Department of Industrial and Materials Science
Chalmers University of Technology
SE-412-96 Gothenburg
Sweden
Tel: +46 (0)31-772 1271
Email: ahmadra@chalmers.se

Printed by Chalmers Reproservice
Gothenburg, Sweden 2021

Abstract

Powder bed fusion (PBF) techniques, including laser-based powder bed fusion (LB-PBF) and electron beam powder bed fusion (EB-PBF), are two rapidly growing additive manufacturing (AM) processes due to their ability to produce complex geometries in near-net shapes. To attain reproducibility and repeatability in PBF processes, a consistent set of powder properties is vital. This is achievable by using virgin powder in every new build cycle. However, considering the amount of unconsumed powder after a build cycle in PBF techniques, reusability of unconsumed powder is imperative to reduce the cost and increase the sustainability of the process. Still, upon reuse the quality of the processed powder gets degraded by surface oxidation or accumulation of by-products often referred to as spatters. The increase in impurities in the powder feedstock can lead to deviation of the powder quality from initial state and cause stochastic flaws in the produced components such as inclusions and porosity. Therefore, it is important to study the powder degradation mechanisms and extent of degradation upon processing to track the changes in quality of powder with reuse. This thesis focuses on analysis of powder degradation mechanisms and their effect on processed components in case of both, LB-PBF and EB-PBF processes.

In LB-PBF process, powder degradation for AlSi10Mg and Alloy 718 powders have been investigated. The examined AlSi10Mg powder was used for over 30 months, and the fabricated parts exhibited an increase in porosity and decrease in tensile strength with increased reuse of powder. The analysis of reused powder samples showed that spatter accumulation is a dominant mechanism in powder degradation. Spatters are an inevitable by-product of the process, and the number of generated spatters depends upon material, process parameters, atmosphere, and geometry of the part. The role of part geometry in spatter generation and powder degradation was further revealed by fabricating specially designed capsules from Alloy 718. Obtained results showed that surface-to-volume ratio and overhang structures tend to increase the number of generated spatters. The analysis of produced Alloy 718 spatters put in evidence the severe surface oxidation with thick Al- and Cr-based oxide patches and particulates formation. By employing an external atmosphere purity system connected to the LB-PBF machine, it was revealed that even if spatters are oxidized particles that can´t be fully avoided, their oxidation can be significantly limited by reducing the oxygen partial pressure in the process chamber. The obtained results showed that spatters generated at <20 ppm residual oxygen content showed only ~30 % increase compared to the spatters generated at 1000 ppm, which showed ~300 % increase in oxygen content. This is a very promising approach to slow down the rate of powder degradation and increase powder reusability for LB-PBF process.

In EB-PBF process, the effect of powder bed oxidation and sublimation of volatile elements from Alloy 718 due to the long-term powder exposure to high temperature and high vacuum level on powder degradation was investigated. It was found that in case of Alloy 718 powder, Cr was dominantly sublimated during the process, which can be detrimental to the superior oxidation and corrosion resistance properties of Alloy 718 components typically preferred for their high temperature performances. Hence, it is important to monitor Cr and Al content both in powder and built parts while processing of Alloy 718 in EB-PBF process.

Keywords: Additive manufacturing; Laser-based powder bed fusion; Electron beam powder bed fusion; AlSi10Mg; Alloy 718; Powder degradation; Oxidation; Spatter particles; Residual oxygen; Sublimation.

Preface

The work presented in this licentiate thesis was conducted at the division of Materials and Manufacture, within the department of Industrial and Materials Science, at Chalmers University of Technology. The work was conducted in the frame of the Centre for Additive Manufacturing – Metal (CAM^2). The research was directly supervised by Prof. Eduard Hryha, and Prof. Lars Nyborg was the examiner.

List of appended papers

I. Degradation of AlSi10Mg Powder during Laser Based Powder Bed Fusion Processing
Ahmad Raza, Tobias Fiegl, Imran Hanif, Andreas Markström, Martin Franke, Carolin Körner, Eduard Hryha
Materials & Design 198(2021) 109358

II. Effect of AlSi10Mg0.4 long-term reused powder in PBF-LB/M on the mechanical properties
Tobias Fiegl, Martin Franke, Ahmad Raza, Eduard Hryha, Carolin Körner
Submitted for journal publication

III. Spatter formation during Laser Powder Bed Fusion of Inconel 718 alloy monitored by Optical Tomography
Zhuoer Chen, Ahmad Raza, Eduard Hryha
Submitted for journal publication

IV. Oxygen balance during laser powder bed fusion of Alloy 718
C. Pauzon, Ahmad Raza, E. Hryha, P. Forêt
Materials & Design 201(2021) 109511

V. Spatter oxidation during laser powder bed fusion of Alloy 718 in dependance on oxygen content in the process atmosphere
Ahmad Raza, C. Pauzon, E. Hryha, Andreas Markström, P. Forêt
Submitted for journal publication

VI. Characterization of spatter and metallization in 718 alloy during electron beam melting process
Ahmad Raza, Eduard Hryha
Submitted for journal publication

Contribution to the appended papers

I, VI: The author planned and conducted the experiments in collaboration with co-authors and wrote the paper in collaboration with coauthors. The co-authors helped in sample collection, TEM and Thermo-calc analysis, and reviewing the articles.

II: The author planned the experiments with the collaboration of co-author as an extension of paper I. The author did the fractography and surface analysis of the powder and contributed to writing of this part. The co-author, Tobias Fiegl, did the rest of experimental work and writing in this paper. The reason of appending this paper is to provide context of paper I.

III: The author planned the experiment with the collaboration of co-authors. Author did the SEM and XPS analysis, and analyzed the results, and wrote that part of paper. Z. Chen did the printing and analysis of OT data and took the lead in writing the paper.

IV, V: The author planned and conducted the experiments in collaboration with co-authors. Author did the XPS analysis and analyzed the results. The SEM analysis was conducted by C. Pauzon. The writing was done in collaboration with co-authors.

ABBREVIATIONS

AM	Additive Manufacturing
BSE	Backscattered Electrons
CAD	Computer Aided Design
CCD	Charge-Coupled Device
EBM	Electron Beam Belting
EB-PBF	Electron Beam Powder Bed Fusion
EDS	Energy Dispersive Spectroscopy
HR-SEM	High Resolution Scanning Electron Microscopy
ALLOY 718	Inconel 718, Alloy 718
LB-PBF	Laser Beam Powder Bed Fusion
PM	Powder Metallurgy
PBF	Powder Bed Fusion
PSD	Particle Size Distribution
RQ	Research Question
SE	Secondary Electron
STL	Stereo-Lithography
STEM	Scanning Transmission Electron Microscopy
XPS	X-ray Photoelectron Spectroscopy

Table of Contents

1 Introduction

1.1 Background

Additive manufacturing (AM) is bringing a paradigm shift in the fundamentals of manufacturing industry from subtraction- to addition-oriented manufacturing. AM was firstly patented by a French scientist Alain Le Mehaute in 1984 [1]. After AM introduction to the industrial world, it was mainly used for prototype fabrication as it reduced the cost and lead time. However, this success is restricted to small batches and mass production has not yet been realized to its full potential [2]. In the last couple of decades, new innovations, both in AM technologies and computation, has made it possible to optimize the products and fabrication time. These advancements making it possible to use AM on larger scales rather than just for rapid prototyping. The major advantages that AM can provide cover: creating products with intricated designs to reduce the material consumption, providing on-site repair possibility to reduce the inventory cost in industry, and cost reduction of the product by producing and finishing at a single fabrication plant [2].

Among AM technologies, metal-based powder bed fusion techniques like laser-based powder bed fusion (LB-PBF) and electron beam powder bed fusion (EB-PBF), have gained a lot of attention both from industry and research community owing to the possibility to produce near-net-shape products with better design accuracy. Particularly, in the field of medical technology, PBF techniques have enabled the engineers to mass produce the implants as well as to fabricate the customized parts with better surface properties, i.e. fabrication of Ti- and TiAl6V4 based implant by EB-PBF process [3,4]. Likewise, products from superalloys (i.e. Alloy 718) fabricated through either LB-PBF or EB-PBF are increasingly getting adopted in the aerospace industry [5–7]. However, there exist several challenges to the adoption of these techniques in the industry. One of these connected to the process sustainability and cost reduction is the reusability of processed feedstock powder in PBF processes [7–10].

In the fields of both research and industry, end-users are mostly relying on virgin (fresh) metal powder for product and process development, and the main reason is to avoid possible consequences related to the degradation of used feedstock. This approach eventually increases the cost of manufacturing and limits its adoption for large-scale production [11]. Still, very little attention has been given to understand the degradation mechanisms of processed powders and its effect on the properties of fabricated parts [12]. To date, the used powders have been preferably studied by evaluation of properties such as flowability, charging and compaction [5,13]. However, powder quality should not be reduced to these process-related aspects, since it was for example shown that rheology may improve with number of reuse cycles and elimination of fines, while powder oxidation increases [13]. This in turn can lead to introduction of nonmetallic inclusions in final products [12], threatening their integrity.

Therefore, a comprehensive understanding of the mechanisms leading to surface chemistry changes upon powder reuse is important. Surface oxidation has been reported to be very dependent on the oxygen affinity of alloying elements. For example Al-, Ti-, and Cr-containing alloys are particularly more prone to oxidation [14–17]. In addition, the nature and rate of powder degradation depends also on the AM process conditions and parameters [7,9,18]. On one hand, in case of EB-PBF, which involves holding the powder bed at high temperatures, general powder bed oxidation plays a dominant role in powder degradation [7,12]. On the other

hand, the LB-PBF process is generally conducted with the powder bed held close to room temperature. Hence, oxidation of the powder bed which is not exposed to the laser radiation is not observed [19]. Still, accumulation of spatters generated by the laser-powder-melt interaction can contribute towards the presence of highly oxidized particles in reused powder for LB-PBF [20–23]. The extent of spatter oxidation in correlation to alloy composition and process atmosphere still needs to be determined.

There are only a few studies available discussing the effect of powder reusability on the extent of oxidation of powder, and thus there is a limited understanding of the powder degradation mechanisms involved during AM. This thesis focuses on the identification of powder and spatter oxidation mechanisms by means of state-of-the-art surface characterization supported by thermodynamic simulation.

1.1 Objectives

The goal of this thesis study is to understand the underlying mechanisms of powder degradation during LB-PBF and EB-PBF processing in correlation to alloy composition. Two materials were covered until now: AlSi10Mg and Alloy 718. To address this topic, an effort has been made to answer the following research questions (RQ):

RQ1: What is the dominant powder degradation mechanism in LB-PBF process?

RQ2: What is the correlation between alloy composition and conditions during LB-PBF processing on spatter formation and properties?

RQ3: What is the dominant powder degradation mechanism in EB-PBF process?

2 Powder bed fusion techniques

Additive manufacturing (AM), also termed as "3-dimensional (3D) printing" is an advanced manufacturing technique where an object is fabricated in additive, layer by layer, fashion [24]. It is a way forward towards the digitalization of manufacturing industry. The digitalization aspect originates from a series of computational pre-fabrication steps that are followed before introduction of design into AM machine and printing. Firstly, the design of component is generated by a computer aided design (CAD) model that contains 2D and 3D graphics of components. The CAD file is then converted to a STL (stereo lithography) file which is triangular representation of surface geometry of the design. The generated STL file is further processed in a suitable AM software to create feasible parameters for printing before transferring to machine. Finally, a machine-readable file containing all the information regarding design, orientation, build direction, support structure, material and process parameters (layer thickness, power, etc.) is introduced to the machine. The process parameters can vary depending on the AM technology. Once all these computational tasks are done, the machine follows the commands and autonomously prints the designed product.

The AM technology can be divided in seven categories as per the ISO/ASTM52900-15 standard of AM. Among the seven categorized technologies in AM, binder jetting (BJ), powder bed fusion (PBF), and direct energy deposition (DED) utilize powder as a feedstock material. The work in this thesis is related to powder bed fusion techniques where metal feedstock powder is used.

Powder bed fusion (PBF) is the dominant AM technology where powder feedstock is melted layer by layer in a desired shape using an energy source. Based on the energy source, PBF can be divided in two processes: laser-based powder bed fusion (LB-PBF) where laser is used to melt the powder layer, and electron beam powder bed fusion (EB-PBF) where an electron beam is used instead. The following sections discuss these two techniques.

2.1 Laser-based powder bed fusion (LB-PBF)

LB-PBF uses laser as an energy source to melt the feedstock powder in the powder bed. The working principle of LB-PBF machine is rather simple and a schematic of the machine is presented in Figure 1. The machine primarily consists of three partitions related to powder: powder dispenser, built area and powder collector [25]. The powder is introduced in the machine by filling the powder dispenser. Once a preset oxygen level is reached in the build area, a recoater rakes a layer of powder from dispenser into the build area. During raking, the overflowing powder is collected in the powder collector. The powder flow from dispenser is controlled by the piston at the bottom of the system which can adjust the available amount of powder. Moreover, the layer thickness is controlled by a piston at the bottom of build area. The position of laser beam is adjusted by using an optical system. After spreading of the powder on the build area, the laser scans the build plate following the component design. Thereafter, this process is repeated layer by layer till the completion of the build cycle.

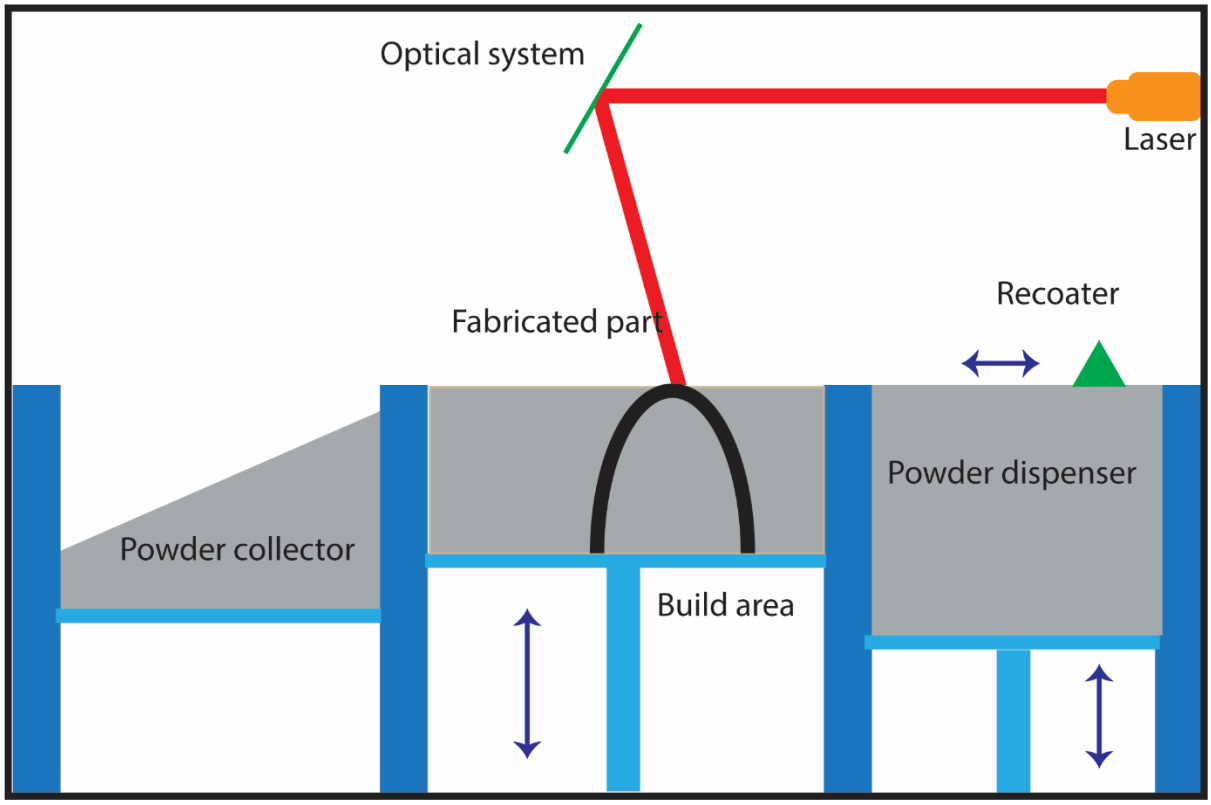

Figure 1: Schematic illustration of the LB-PBF machine while laser scanning.

After the build process is completed, the unconsumed powder is removed by a powder extraction module and sieved to eliminate spatters and debris before further reuse. Used sieve size depends upon the powder size distribution (PSD) of virgin powder. After powder removal, the build platform is moved from machine for post processing. The post processing can consist of various steps including support removal, machining, surface treatment, etc. The homogeneity of post processing after each build is important to achieve the reproducibility in the properties of fabricated parts. Additionally, several other parameters can substantially influence the properties of fabricated parts including powder quality, powder size distribution (PSD), laser power, layer thickness, hatch distance, scan speed, scan strategy, gas flow rate etc. A careful control of these parameters is vital to achieve reproducibility of LB-PBF products.

2.2 Electron Beam Powder Bed Fusion (EB-PBF)

The EB-PBF is an AM technique which enables the production of multilayer components without any support structure, unlike LB-PBF. Figure 2 is showing a schematic of EB-PBF machine which has hoppers on both sides of the build area. A recoater is used to take the powder from hoppers and spread it in the build area after each printing cycle [26]. As it is given from the name, the heat source is electron beam, where the beam direction is controlled by electromagnetic lenses. The beam control from electromagnetic lenses makes EB-PBF process manyfold faster than LB-PBF process. To achieve the high energy efficiency, ultrahigh vacuum ($\sim 10^{-6}$ bar) is a prerequisite for EB-PBF process [27].

The electron beam scanning of the powder bed works in two steps. The first step consists of the scanning of the whole powder bed to heat it to a sintering temperature where powder can be semi-sintered. Sintering of the powder is important to increase the conductivity of the powder-bed. Un-sintered powder can cause accumulation of electrons due to poor powder bed

conductivity, and result in ejection of powder from powder bed by repulsion before melting, an effect commonly known as smoking effect in EB-PBF technology. The semi-sintering of powder at elevated temperature has some additional benefits other than avoiding smoking effect: the support structures can be avoided/minimized as the sintered powder act as support. It also permits to avoid the generation of residual stresses. During the second step, electron beam of high energy selectively scans the designed part where the system increases the beam energy to melt the sintered powder bed. This process is repeated until the build height of the fabricated part is reached.

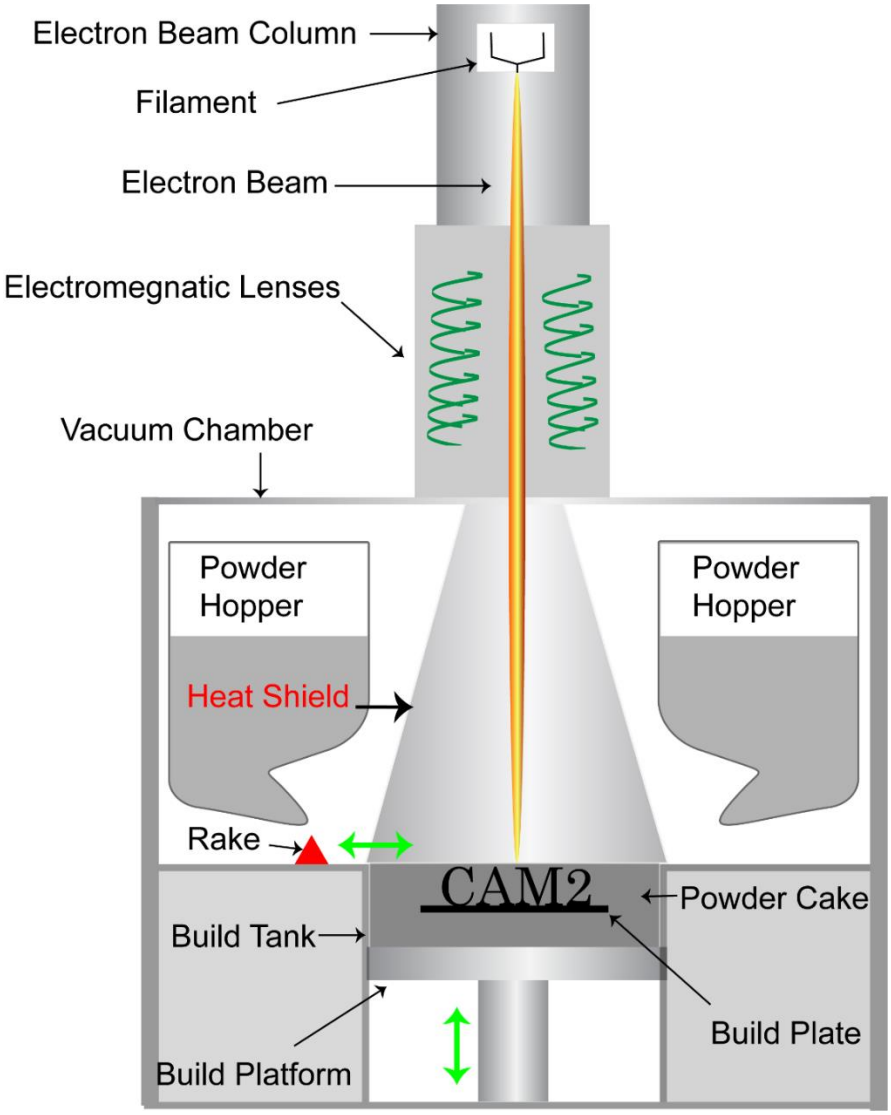

Figure 2: A schematic illustration of EB-PBF process.

After the completion of a build cycle, the machine is allowed to cool down before opening the chamber to avoid oxidation of unused powder. After cooling, the build platform containing the powder cake is removed from the machine and placed in a powder recovery system. To separate the sintered powder from fabricated components and the cake itself, grit blasting is conducted. Grit blasting assists in converting the semi-sintered cake into powder particles for further reusability after sieving. Moreover, the retrieved components go through further post processing before being used in required applications.

Though high temperature and high vacuum improve the stability of the process, these prerequisites can increase the rate of powder degradation. These aspects are further discussed in the following chapters.

3 Powders for Additive Manufacturing

Around 5000 alloys and metal systems are available in conventional metal related industry [28]. Being an emerging field, such a wide range of metallic material options are not available yet for AM. The usage of already existing alloys in AM still requires a complex material/process development where the interaction of energy source with powder in build environment needs to be comprehensively understood. Due to the complexity of process development, only 30 metal alloys are qualified to be used in powder based AM techniques (PBF, BJ, and DED) [28], see Table 1. Although most AM materials (presented in Table 1) are adopted from conventional alloys, the composition requires tailoring of most of alloys to adapt to rapid melting and solidification nature of AM process. This composition tailoring is also part of complex material development for AM technology.

Table 1: List of qualified powder-based metal AM techniques

AM technology		Alloys	No
PBF	**LB-PBF**	Al: AlSi10Mg, AlSi7Mg0.6, AlSi9Cu3, AlSi12, Scalmalloy Co: CoCr28Mo6, CoCr24Mo5, CoCr25Mo5W5 Cu: Cu, CuCrZr, Cu-10Sn, CuNi2SiCr Ni: IN625, IN718, IN939, HX Ti: TiCP, Ti6Al4V Stainless steel: 316L, 17-4 PH, 15-5PH Tool steel: CX, PH1, GP1, 20MnCr5, MS1, 1.2709, H13 (1.2344), Invar36 Refractory: W Precious: 18714K Gold (red, yellow, white), 925Si, 95Pt/5Ru	33
	EB-PBF	Ti: Ti, Ti6Al4V Co: CoCr28Mo6 Ni: IN718 Intermetallics: TiAl4822	5
BJ		Ni: IN625, 247 Ti: Ti6Al4V Stainless steels: 316L, 17-4PH, 304L Tool steels: M2	7
DED		Ni: IN625, IN718 Ti: Ti6Al4V Stainless steel: 316L	4

Despite the limited number of metallic materials for AM, they cover a wide range of compositionally different alloys with varying physical properties and chemical activity. Therefore, the adoption of powder manufacturing route requires a careful consideration of alloy composition and intended chemical, and physical properties of powder. In following sections, powder manufacturing methods for AM will be presented. Furthermore, the required set of powder properties to be considered for powder use in AM will also be discussed.

3.1 Powder manufacturing methods

Powder fabrication for powder metallurgy techniques is a well-established field, and several techniques are being used to produce the powder from bulk material. Such techniques involve mechanical comminution, chemical reduction of brittle materials, electrolytic reduction from solution, disintegration of liquid melt. For metal powder fabrication, physical disintegration of

liquid melt is the most utilized technique industrially, and this process is called atomization [29–32].

Powder fabrication for AM requires additional attention as powder shape, size, morphology, surface chemistry, rheology, etc., can potentially influence the processability of powder in AM machine. The following atomization techniques are commonly used for powder production for AM:

1. Inert gas atomization
2. Electrode induction gas atomization (EIGA)
3. Plasma atomization process
4. Plasma rotating electrode process

3.2 Inert gas atomization

Gas atomization is the most used atomization technique for AM powder production, particularly for Fe-based (stainless steels, low and high alloy steels etc.) and Ni-based (Hastelloy X, IN625, Alloy 718 etc.) alloys [33]. A schematic illustration of this technique is presented in Figure 3a. In first technique (shown in Figure 3a), virgin raw material is charged in the induction furnace which uses the eddy currents to melt the material [31]. Depending on the susceptibility of alloying elements for oxidation, the furnace is placed in vacuum, inert or open-air environment. The melt is overheated to compensate the heat loss in subsequent steps. In next step, the melt is transferred to tundish for even flow of the melt to atomizer nozzle. Once the melt passes the nozzle, a pressurized gas disintegrates the melt stream into fine melt droplets. These melt droplets get solidified during their time of flight before settling at the bottom of atomizing chamber. During solidification, the surface tension of the droplet pulls it into adopting a spherical shape to minimize its surface energy.

Within this method, there are two types of atomizing nozzles commonly used: freefall nozzle, and close coupled nozzle. The type of selected nozzle can influence the produced powder size and morphology. For a close coupled nozzle, powder size distribution (PSD) lies in the range of 5-200 μm with D50= 50 μm. While with a free-fall nozzle, PSD achieved is in the range 50-300 μm with D50=100 μm [28]. Although the close coupled nozzle produces finer range of powder, there exist a higher possibility of satellite formation on powder surface due to the turbulent flow of melt in the nozzle.

3.3 Electrode induction gas atomization

Electrode induction gas atomization (EIGA) is a variation of inert gas melting in terms of charging method where a bar with fixed composition is melted by induction. The typical diameter of charged bar is up to 150 mm. The melt flows through an atomizing nozzle and get disintegrated to fine droplets, see Figure 3b. These droplets solidify during the time of flight and settle at the bottom of chamber. The PSD of produced powder lies in the range of 10-500 μm with D50=90-140 μm. This process is more common in alloys which contains highly reactive elements as TiAl6V4, TiAl, NiTi etc. to avoid oxide impurities.

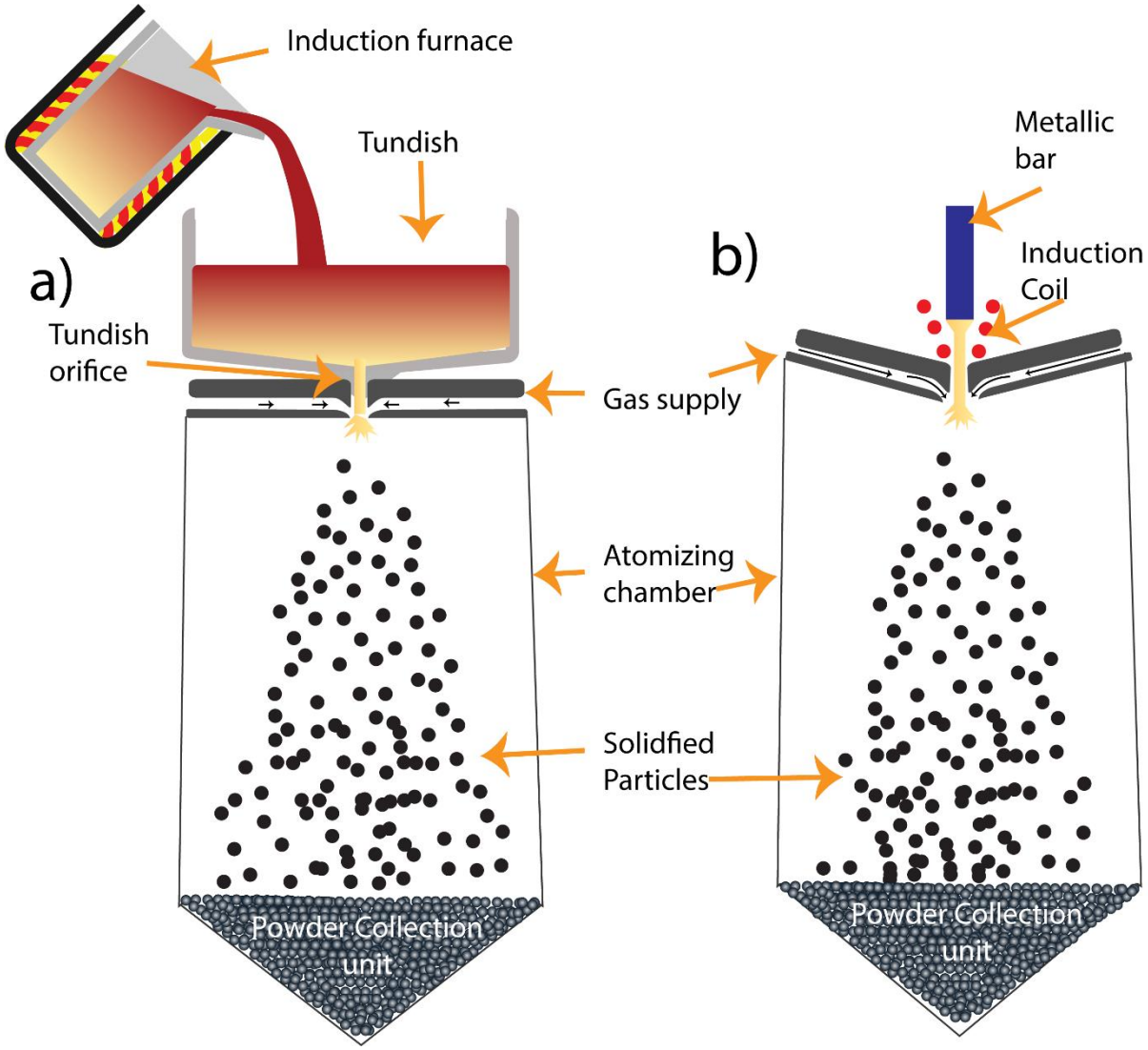

Figure 3: A schematic of gas atomization process with charging through a) induction furnace, b) electrode induction melting.

The micrographs presented in Figure 4 elucidates the difference between the quality of powders produced through conventional gas atomization and EIGA of Alloy 718. Due to a controlled gas and melt flow, finer particle size distribution can be achieved by gas atomization, see Figure 4a. However, a turbulence in the melt flow can cause the formation of finer particles which solidify quickly and land on the surface of coarser particles in the form of satellites. Contrarily, in EIGA, gas jets can directly interact with the melt stream coming from the electrode due to the geometry of the free-fall nozzle. Here, the distance between melt stream and gas jet nozzle is higher which dissipates some of the energy of gas jets before interacting with the melt stream. This results in coarser size with the EIGA process. Yet the powder has a higher sphericity and cleaner surface without any satellite presence, see Figure 4b.

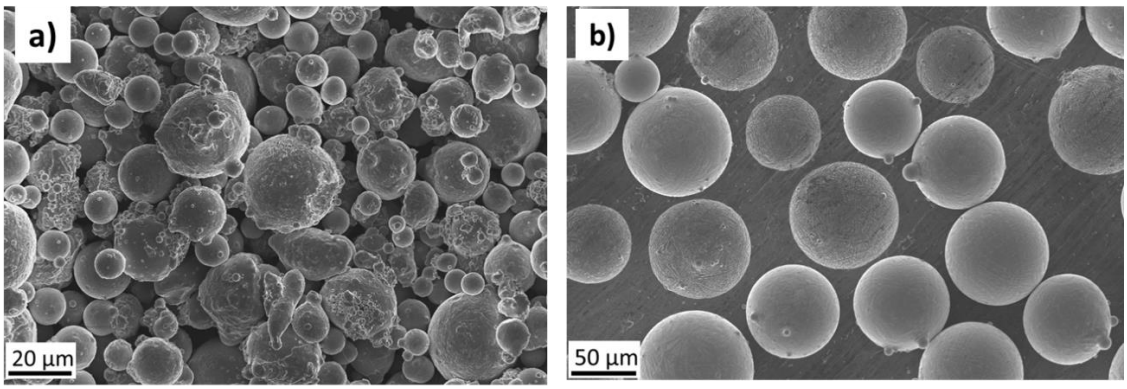

Figure 4: Morphology comparison of powders produced through a) conventional gas atomization (GA) and b) electrode induction gas atomization (EIGA).

3.4 Plasma atomization process

The plasma atomization process uses the plasma torches as heat and atomization source and wire as feedstock material [34], see Figure 5. The plasma interacts with the wire, melts it, and atomizes the melt. The melted droplets get solidified and collected like in conventional gas atomization process. The produced powder through this technique usually exhibits high sphericity with cleaner surface. However, there exist challenges with this process. The production rate is very slow which exponentially increases the cost of process. There is no possibility to change composition during atomization as the feedstock material needs to be in form of wire. The PSD of powder produced through this technique lies in the range of 0-150 µm with D50= 40 µm. This technique is mainly used to produce powders from Ti alloys as well as number of other advanced materials when high powder sphericity and purity are required, which are difficult to handle by gas atomization.

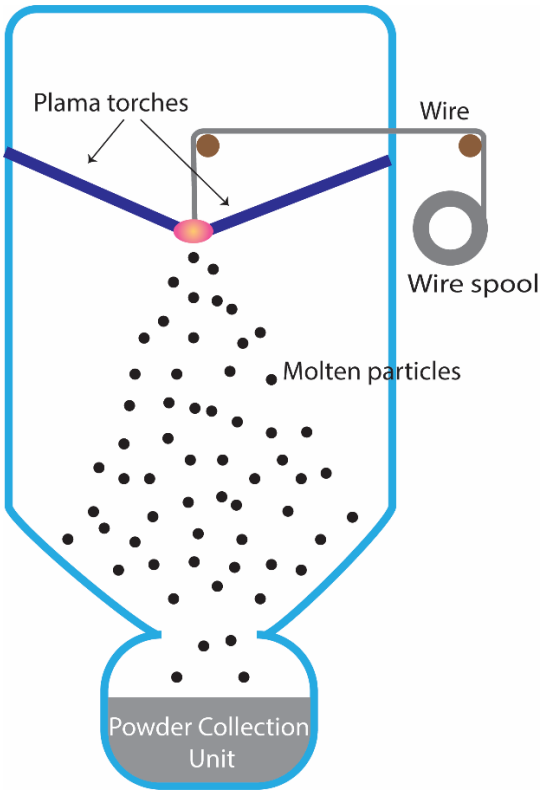

Figure 5: A schematic of plasma atomization using metal wire as feedstock.

3.5 Plasma rotating electrode process

Plasma rotating electrode process allows to produce high quality metallic powders in terms of sphericity and surface cleanliness [32]. In this process, a metallic electrode is mechanically rotated and the end of this electrode is melted by a plasma torch, see Figure 6. The liquid metal flies off by centripetal force and solidifies into a perfect spherical shape. Historically, this process was used to produce coarse PSD. However, with adoption of AM, new modifications in the process have been developed where the increase in rotation speed of electrode can assist in producing suitable PSD for AM. This technique is used to produce high quality powder for fabrication of critical components through AM.

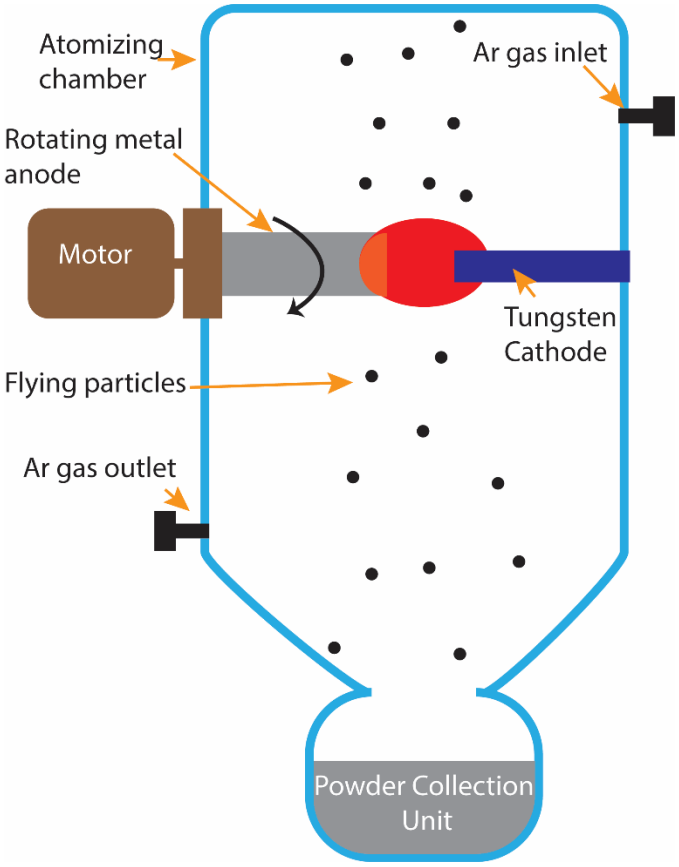

Figure 6: A schematic of plasma rotating electrode process.

3.6 Powder properties for additive manufacturing

For successful fabrication of AM products, powder properties optimization is an essential consideration and remains a challenge for the researchers [35]. Powder properties influence both the interaction of powder with AM systems and bulk properties of final product. As for example powder morphology can affect the density of powder bed (in PBF techniques), surface roughness, melting/sintering kinetics and density of manufactured part, etc. [36]. To achieve the repeatability and reproducibility, it is important to control the powder properties. Therefore, there is a need to standardize the required aspects which should be considered before introducing the powder into the machine. Figure 7 portrays the important powder properties which should be studied to evaluate the status of powder. Rheology, density, and morphology are process related aspects of powders and assist to predict the processability of powder in AM; whereas chemistry and microstructural properties are concerned with the metallurgical quality of powder.

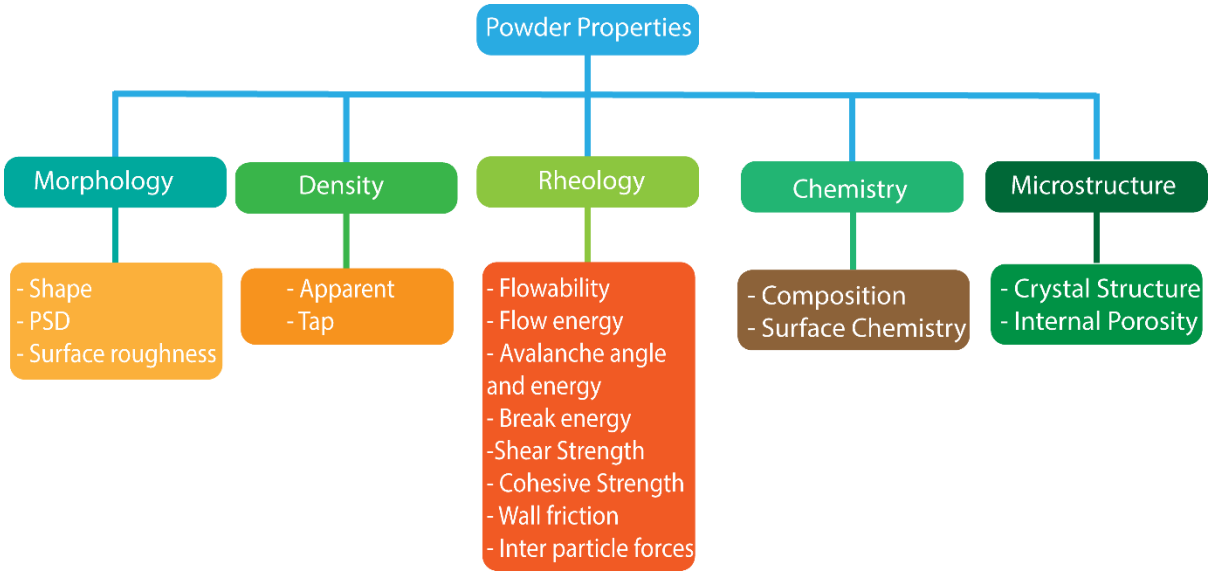

Figure 7: A tree diagram representing the important powder properties for AM.

State of the art research regarding powder properties is mostly focused on powder morphology and rheology. In term of reusability, the quality of powder is often determined by analyzing the variation of PSD and flowability [13]. Cordova et al. [13] have done a comprehensive analysis of TiAl6V4, Alloy 718, AlSi10Mg, and Scalmalloy powders to determine the effect of powder reusability on PSD and flowability. The results showed a slight increase in PSD, particularly for AlSi0Mg and Alloy 718, which can be controlled by implementing proper sieving after each build. Further, the results showed that the flowability improved in reused powder compared to that in virgin powder due to the loss of fine particles during reusability. Additionally, the bulk chemical analysis showed an increase in oxygen content for AlSi10Mg alloy due to the high affinity of Al for oxidation. This is the only detrimental aspect found in the analysis after reusability. Sutton et al. |37] also showed similar findings regarding PSD, flowability, and oxygen pickup while reusing AISI 304 L alloy powder for 7 build cycles. Hence, rheology (which improved in reused powder) and PSD (which can be controlled by sieving process) can only help in determining the processability of powder in PBF machine, and not the quality of powder and how it can affect the properties of produced components. Hence, there is a need of process development to evaluate the quality aspect of powder during reusability, which can be done by a dedicated chemistry analysis.

The chemistry analysis can be divided into two subcategories: bulk composition and surface chemistry. Bulk composition analysis is a swift way to know the change in composition from virgin to reused powder considering surface and bulk chemistry of the particle. In most of the cases, this change will result in increase of oxygen content by oxygen pickup during process. However, this information needs to be complimented with a detailed surface analysis to know the distribution of oxygen on powder surface, main oxide forming elements, and change in oxide layer thickness. Understanding of oxide type and oxide layer thickness is vital to know their behavior during laser-powder interaction and in the melt pool (whether the oxide will dissolve, mix or float), and develop models for powder degradation during AM. Furthermore, the identification of dominant oxide forming elements in each alloy can indicate depletion of critical elements in bulk (e.g., Al in Alloy 718).

4 Powder degradation in PBF techniques

4.1 Thermodynamic Analysis

This section introduces basics of thermodynamics allowing us to understand the preferential stability of various oxides. Important consideration here is that most of these calculations are for equilibrium conditions, which are drastically different from the actual conditions during oxide formation on powder exposed to the AM environment (especially during oxidation of spatter particles). However, they provide indication to understand the likeliness of certain oxides formation in complex compositions. The principal concept behind the calculations of driving force is the change in free energy (ΔG) for the reaction from metal to oxide state, derived from following equation:

$$\Delta G = \Delta H - T\Delta S \qquad (1)$$

Here, ΔH is the enthalpy change, ΔS is the entropy change, and T is the temperature in Kelvin degrees. In oxidation, considering their exothermic nature, the ΔG results in negative value. In such scenario, the preferred oxidation of elements in alloys with complex composition is a big consideration. For example, in a simple alloy like AlSi10Mg, all three main alloying elements have strong susceptibility for the oxidation, but there is a preferential oxidation of Al and Mg compared to Si in the sense that the strongest oxide former will react first with oxygen provided that there is no kinetic constraint.

Additionally, Figure 8 showing the Ellingham diagram from which is a collection of standard free energy changes ΔG^0 for the formation of oxides form their elements is shown as a function of temperature (T). At equilibrium ΔG=0, and the standard free energy change can be expressed by following equation:

$$\Delta G^0 = -RT\ln(K) \qquad (2)$$

Here, K and R are the equilibrium constant and gas constant respectively. For oxidation/reduction reactions, considering the pure elements and the respective oxide forming, this equation can be expressed as:

$$\Delta G^0 = -RT\ln(pO_2) \qquad (3)$$

The Ellingham diagram is very useful to determine the oxide stability with increase in temperature and partial pressures of various gases e.g., pO_2, pH_2/pH2O and pCO/pCO2, where the latter two equilibrium ratios are simply derived from the oxidation of H_2 to H_2O and from CO to CO_2. Although Ellingham diagram can assist in predicting the possibility of reaction, it cannot tell the rate of reaction. For that, other kinetic considerations (diffusion rate etc.) need to be used.

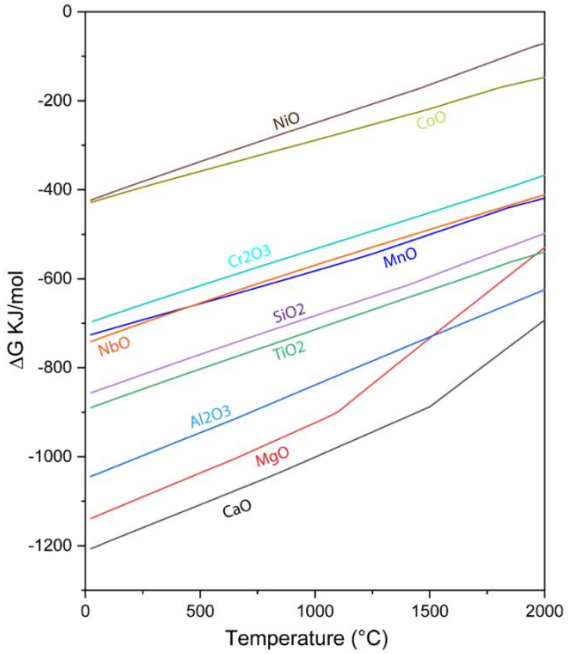

Figure 8: Ellingham diagram showing a change in Gibbs free energy with respect to temperature. The graph is acquired using HSC 9.0 software.

The CALPHAD method [38] is a well-established technique for assessment and calculation of thermo-chemical information and phase equilibria for multi-component systems. In present thesis we have used Thermo-Calc 2021a. In this respect the actual impact of activity of elements can be considered and possible formation of complex oxides can be modelled. In conjunction with suitable thermodynamic databases, assessed using the CALPHAD approach, Thermo-Calc can be used for a wide variety of applications. For analyzing the oxide formation behavior, TCOX10 [39] database was used. In addition, for kinetics and diffusion calculations, the MOBNI5 (Ni-Alloys Mobility v5.1) database along with diffusion module DICTRA in Thermo-Calc can be used.

Another important aspect of thermodynamic calculations is sublimation/evaporation of various elements, particularly in EB-PBF process. EB-PBF process operates at elevated temperatures and high vacuum levels, which give a rise to the evaporation of certain elements. As the rate of evaporation is not same for elements, sublimation can result in modified composition of the processed alloy. The HSC 9.0 software is a useful tool to calculate the vapor pressure of various elements and oxides at elevated temperature for high vacuum conditions.

4.2 Surface chemistry of powder

Surface area of normally used AM powder is ~10,000 times larger than bulk material of same mass [40]. This results in substantially high surface reactivity of metallic powders which enables it to form surface oxides. Still, it should be noted that the thickness of ambient oxide may not necessarily be much greater than that of technical flat sample. The high specific surface are and the presence of oxides on powder surface and their subsequent inclusion in manufactured components can be though detrimental for mechanical properties of fabricated parts. It is well known from sintering process that the presence and thickness of oxide layer can influence the process dynamics and properties of the final component [41]. Therefore, it is important to depict the thickness and nature of oxide layer on the powder surfaces. This section

aims to introduce the surface analysis tools, dependance of surface oxidation on composition and atomization route and powder degradation in AM.

To understand the surface chemistry of metallic powders, Olefjord and Nyborg [42] began using surface sensitive techniques, such as X-ray photoelectron spectroscopy (XPS) and Auger electron spectroscopy (AES) in 1980s. Due to higher surface sensitivity, these techniques provided a comprehensive information regarding the nature, thickness, and dominant oxide forming elements on the powder surface. In one of their earlier works on gas-atomized steel powder, Olefjord and Nyborg [43] were able to provide the specification of surface oxides, area coverage by certain oxide particulates compared to total surface area and thickness of oxide layer. Thereafter, this technique has become a routinely used tool to analyze the surface chemistry of metallic powder.

Nature and stability of surface oxide depends on the composition of powder and conditions of its fasbrication and storage. Enoughpresence of stable oxide forming elements in composition, such as Al, Ti, Cr etc., can effectively hinder the powder surface oxidation after initial uniform protective oxide layer formation. One such study was conducted by Hryha et al. [44] where they compared a virgin NiTi powder with the same kind of powder that was stored for up to 8 years. The comparison of oxide layer thickness of fresh powder with the powder stored for 8 years showed that there was only 15% increase in oxide layer thickness owing to the passive nature of oxide film. Hence, composition of alloy has a decisive role in determining the nature and thickness of oxide layer on the powder surface. Besides, atomization route can also strongly influence the type of oxide formation on powder surface. Riabov et al. [33] did a comparative surface analysis on 316L stainless steel powder produced through vacuum induction-melt gas atomization (VIGA), air melted gas atomization (GA) and water atomization (WA). Oxide particulates enriched with Cr and Mn were found on the surface of powders produced through both VIGA and GA. Overall coverage of oxide particulates on the powder surface was similar for both VIGA and GA, except for the presence of a additional small amount of Si-rich oxide particulates in GA. However, the surface of WA powder had higher coverage by oxide particulates of stable oxides compared to VIGA and GA. The oxide particulates was now enriched with Cr and Si. In short, both the composition and powder manufacturing route can influence the nature and type of oxide present on powder surface [33].

Lastly, in PBF techniques, it is important to reuse the unconsumed powder to increase process sustainability and reduce cost. However, there exist a possibility of further powder degradation besides initial surface oxidation (during powder atomization) by powder exposure in machine environment and accumulation of process by-products [40]. Reuse of degraded powder can leads to oxide inclusion and other defects in produced components [17][45]. Therefore, it is essential to develop the understanding of powder degradation mechanisms in powder bed fusion techniques. Following chapters will elaborate on various powder degradation mechanisms in LB-PBF and EB-PBF processes.

4.3 Powder degradation in LB-PBF

In laser powder bed fusion, there are two main mechanisms which can possibly contribute towards the degradation of unused powder in powder bed: surface oxidation and spatter formation.

4.3.1 Surface Oxidation

Powder surface oxidation is commonly known phenomenon in powder technology owing to high surface to volume ratio. Especially, the alloys with the elements like Al, Cr, Ti, Zr etc., which are highly susceptible to oxidation, are vulnerable to surface oxidation [46–48]. However, there exist a positive aspect in LB-PBF technology that the powder bed is kept in inert atmosphere and in proximity of ambient temperatures [49]. Once a uniform oxide layer forms on the powder surface, it passivates and hinder further oxidation. A study conducted by Quintana et al. on the reusability of TiAl6V4 powder showed a mere 30% increase in oxygen content in reused powder after 31 reuse cycles ($\sim 600h\ machine\ time$) [50]. This stability was stemmed from the stable TiO_2 layer formation which inhibited further oxidation of the powder. In a similar study on Alloy 718 by Ardila et al. [19] found no noticeable change in chemistry of reused powder compared to virgin powder. From these studies, it can be concluded that the in-process oxidation of unconsumed powder in the bed (which is not affected by laser beam) is not a dominant powder degradation mechanism in LB-PBF process.

4.3.2 Spatter Formation

Spatter formation and accumulation in powder bed could be a dominating powder degradation mechanism in LB-PBF process [51]. Spatters are by-products of LB-PBF process, which forms by laser-melt-powder interaction. All the ejections by laser-melt interactions are not the same, and spatters can vary in size, shape, morphology and chemistry, individually [23,52]. These variations are linked with the generation mechanism of spatter particles. A schematic of LB-PBF process is shown in Figure 9 highlighting the commonly ejected particles by laser-melt-powder interaction. The color of ejecting powder particles represents the difference in temperature and origin of spatter particles. Firstly, the melt pool ejecta is the molten material, ejected from melt pool due to recoil pressure [20,53]. This molten ejection can either solidify during the time of flight and land on powder bed or coalesce with other ejecting particles and form bigger particle [54]. However, if this ejected melt land on powder bed before solidifying, they could form agglomerates with the pre-existing powder. Secondly, the cold spatters can be ejected by impact of metallic vapors or entrained by low pressure zone (prior to interaction with laser) [55]. In contrast to cold spatters, some entrained particles can interact with laser during ejection and appear as hot particles. Such hot particles can usually be in partially molten state or have temperature near to the melting point [55]. Since spatters have different origin (and thus thermal history) they are likely to undergo different rates of oxidation.

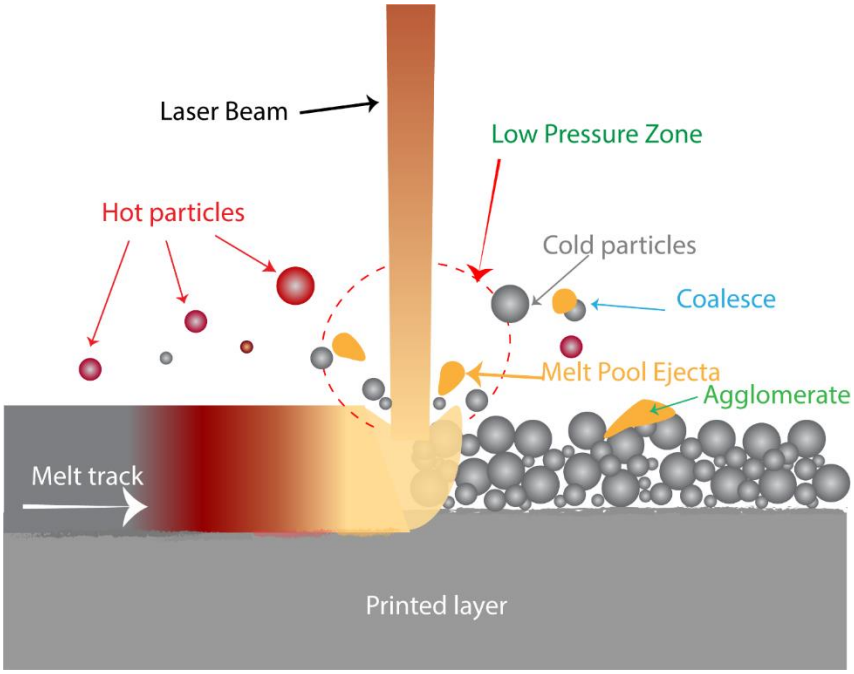

Figure 9: A schematic showing spatter formation in LB-PBF process.

Numerous factors can influence the generation of spatters which includes beam energy density, beam size, scan speed, material, processing gas and its purity. Correlation of materials effect on spatter generation was studied by Gunenthriram et al. [21] where they compared the spatter generation rate in 316L and AlSi10Mg alloy and found that 316L stainless steel generated higher number of spatter compared to Al12Si alloy. The proposed reason was the low upward trajectory of Al12Si spatters, which assisted in incorporation of ejected particles in melt pool. Regarding the effect of processing gas, Pauzon et al.[51] compared the Argon (Ar), Helium (He), and mixture of He and Ar gases. The finding evidenced that the hot spatters can be reduced by up to 60% in He gas, and by 30% in mixture of the gases, whereas the number of cold spatters was same in both cases. Furthermore, due to higher thermal conductivity of He gas, higher cooling rate of hotter spatters was observed in He gas environment compared to in Ar gas. However, there exists a niche to evaluate the effect of part geometry on spatter generation, which is assessed in this thesis.

Spatter formation can affect the build quality in multiple ways. Firstly, the spatters can interact with laser beam during time of flight and attenuate the beam resulting in a discontinuity in energy input to the built layer, which can result in a defect [51]. Secondly, the redeposition of spatters on powder bed can negatively influence the component properties by changing the layer thickness of powder bed. Thirdly, accumulation of such particles can influence PSD, morphology, and flowability of powder which can negatively influence the properties of fabricated parts [20]. Lastly, mass transfer of elements with high oxygen affinity can occur in hot spatters. Such particles can get oxidized and their accumulation in powder bed can increase the overall oxygen content in powder bed. This can result in a possibility of oxide inclusion formation in the produced component, and local discontinuity of energy absorption (change in energy coupling between energy source and powder). Also, the oxidation behavior of spatters can vary from material to material, which makes it important to analyze the oxidation behavior of spatter particles by a dedicated surface analysis.

4.4 Powder degradation in EB-PBF process

EB-PBF process operates at elevated temperature (650-1050 ^{o}C). These temperatures are quite high to accelerate the surface oxidation of powder by mass flow of elements with high affinity for oxygen from core to the surface of the particle. Several researchers have reported their findings regarding oxygen pickup during EB-PBF processing of TiAl6V4 and Alloy 718 [56]. In a study by Nandwana et al. [57], gas atomized TiAl6V4 powder was analyzed. The results showed a linear increase in oxygen content from 0.14 wt. % to 0.18 wt. % in five cycles. In a similar work on TiAl6V4, Ghods et al. [58] also showed a linear increase in oxygen content for grade 5 TiAl6V4 from 0.14 wt. % in virgin to 0.20 wt. % after 11 cycles. However, Shanbhag et al. [59] observed a rapid increase from 0.13 wt. % to 0.17 wt. % in grade 5 TiAl6V4 powder in just two cycles. Additionally, for Alloy 718, Nandwana et al. [57] observed an increase in oxygen content from 0.014 wt. % to 0.022 wt. % after 6 cycles. For same alloy, Gruber et al. [7] observed an increase in oxygen level from 0.0146 wt. % to 0.0266 wt. % after 14 cycles of reuse. From these findings, it can be concluded that powder oxidation is a dominant degradation mechanism in EB-PBF process owing to extremely high process temperature. However, there exist an inconsistency in reported research regarding the rate of oxidation for both TiAl6V4 and Alloy 718.

Such inconsistencies can be linked to the operator's skills and powder handling atmosphere. A careless handling of machine by operator can incur impurities in the form of residual hydrocarbons in the chamber [56]. Also, a leakage in system can cause the permeation of water molecules into the EB-PBF chamber, which is less likely with better vacuum sealing [56]. Both these factors can increase oxygen impurities in processing chamber and result in higher oxygen pickup rate. Additionally, humidity in powder handling atmosphere can also influence the oxygen pickup rate. Nandwana et al. [57] has reported that main source of oxygen contamination in EB-PBF chamber is adsorbed water on the powder surface. Such adsorption happens during air exposure of powder (during sieving and storage). Processing in a humid environment can increase the adsorbed amount of water on powder surface and results in higher oxygen pickup rate and vice versa. Furthermore, Powder handling in air atmosphere can also lead to the formation of Ni and Fe based oxides/hydroxides [7]. These oxides are unstable at high temperature and can redistribute the oxygen to stable oxide forming elements, which then results in increased amount of stable oxides [7]. Hence, combination of all the process variations can cause the inconsistency in rate of powder oxidation in EB-PBF process.

Additionally, oxidation tendencies and nature of oxides can differ in different alloys. In a study on Alloy 718, Gruber et al. [7] analyzed the surface evolution of powder while reusing it for 30 build cycles. The findings showed that the oxide formation on powder surface is not uniform. It is rather in the form of Al-based oxide particulates. Amount and coarseness of such oxides increased with the number of reusability cycles. Formation and stability of Al-based oxides is linked with most negative ΔG^{o} value of Al_2O_3 compared to those of Ti, Cr, Fe, Ni oxides, see Ellingham diagram in Figure 8. Also, Al_2O_3 has higher stability in EBM conditions, and it acts as a reducing agent for the oxides of other elements, see Figure 10. Figure 10 highlights that presence of any Ni, Fe based oxide/hydroxides, by air exposure of powder, will result in redistribution of oxygen to more stable oxide forming elements such as Al, Ti, Cr, etc.

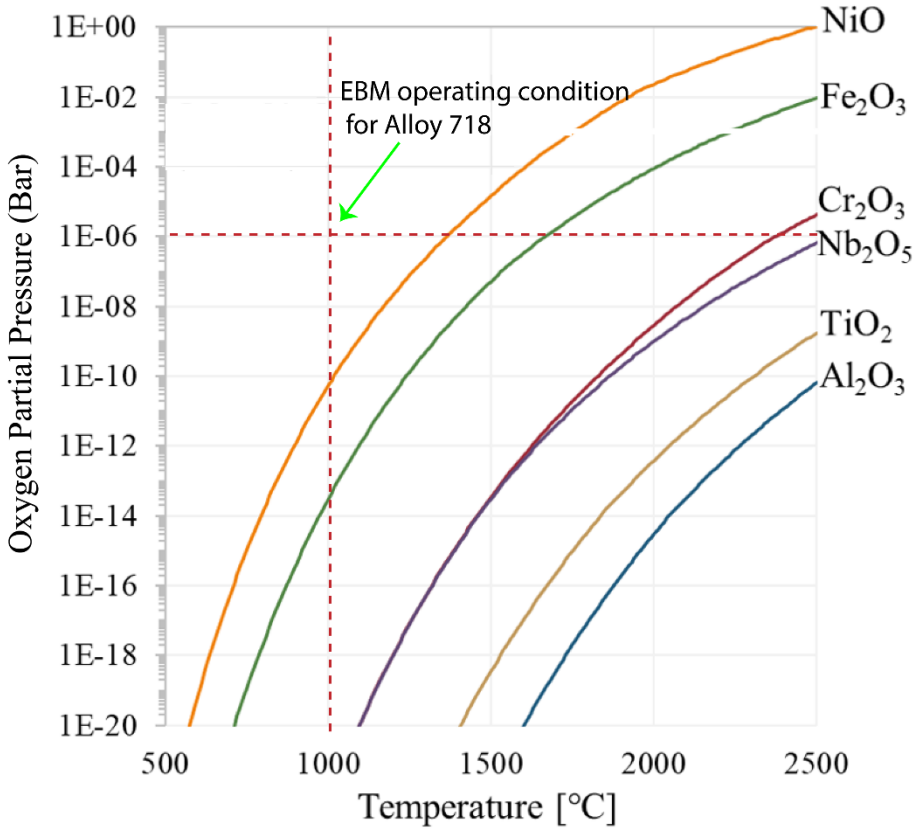

Figure 10: Equilibrium oxygen partial pressure for some elements in oxide form of Alloy 718.

Contrarily, processing of TiAl4V6 in EB-PBF process showed the formation of a uniform oxide layer, by Sun et al. [60]. These authors found that the thickness of oxide layer remained below 10 nm even after 30 reuse of cycle and 35 % increase in average powder oxygen content. The additional amount of oxygen enriched the β phase. Montelione et al. [11] also showed a continuous increment in oxygen content without a significant change in oxide layer thickness. Hence, tendency to oxygen pickup varies depending upon the composition of alloy, and it is important to analyze the oxidation behavior of powder and assess the factors which are contributing towards accelerated oxidation. It should be noted that Ti per se has high solubility for oxygen in its alfa phase and hence in some way can be its own getter material in vacuum condition.

4.5 Sublimation of metallic elements during EB-PBF

Given the high vacuum and high temperature as the main prerequisites of EB-PBF process, these conditions can accelerate the sublimation of elements with higher vapor pressure as e.g., Al and Cr [61]. Particularly, in alloys like TiAl and TiAl6V4, the sublimation of Al is very prominent and commonly observed. In an earlier study on TiAl, an up to 7 at. % decrease in Al content was observed from the virgin powder to the fabricated parts [62]. In another study by Petrovic et al.[63] on TiAl6V4, they observed a 3% decrease in Al content after 12 reuse cycles. Hence, sublimation is also a critical aspect to be considered in EB-PBF process. There are a few recent studies on process optimization to reduce the rate of sublimation from the melt pool. A study by Schwerdtfeger et al. [64] on the optimization of layer thickness and overall volumetric energy density while processing Alloy 718 allowed to reduce the change in built

sample from the virgin powder to 1.5 at. %. In an additional study, Damri et al. [65] suggested an increase in pressure of built chamber by one order of magnitude (from 10^{-3} mbar to 10^{-2} mbar), which didn't significantly affect the energy efficacy of beam, but can help to reduce the evaporation of elements.

5 Materials and Methods

This chapter includes the materials used in the studies presented in this thesis along with the characterization techniques used for analysis.

5.1 Materials and processing

The studies presented in this thesis includes the work on mainly AlSi10Mg when processed by LB-PBF and nickel-based superalloy Alloy 718 when processed by LB-PBF or EB-LBF. Following paragraphs details the materials, processing, and sampling method for analysis.

5.1.1 AlSi10Mg

Owing to its good castability, weldability, corrosion resistance and hardenability, the AlSi10Mg alloy is being commonly researched for optimization for component properties in LB-PBF process [5,13]. It is a near eutectic alloy of Al-Si where the introduction of Mg can cause precipitate formation of Mg_2Si to strengthen the matrix without any detrimental effect on the mechanical properties of the alloy.

Here, the AlSi0Mg alloy powder, provided by Concept Laser GmbH, with nominal composition Si 10.1 wt. %, Mg 0.4 wt. % and Fe 0.11 % balanced with Al was investigated. Particle size distribution in virgin powder was in the range of D10= 45 μm, D50= 65 μm, and D90=93 μm. The powder was produced using gas (nitrogen) atomization, the resulting powder has a nearly spherical shape with satellites attaching on the surface of the powder. The satellites are the fine particle with size < 5 μm generated during atomization and adhered on the surface of larger particles.

5.1.1.1 LB-PBF processing of AlSi10Mg

For LB-PBF processing of the powder, XLINE 2000R Concept Laser GmbH machine is used with the build chamber size of 800 x 400 x 500 mm^3. The machine has a built-in sieving station and silo system which is interconnected with the build chamber, which assists in maintain the same controlled inert environment while reusage of the powder [66]. Both the build chamber and sieve station are flooded with fresh nitrogen gas to keep the oxygen level below 1000 ppm in the chamber. The powder remains in the inert environment except the time when the build chamber is opened at the end of build job to remove the build plate. During the removal of build plate, the unused powder gets exposed to the open environment for a few minutes. The unused powder from build plate is extracted in inert atmosphere in the glove box. From glove box, the powder is transported to the sieving station through interconnected pipeline. The sieving station sieve the powder to maintain particle size distribution like virgin powder to enhance the reproducibility in the properties of the products.

The system operates with approximately 550 kg of AlSi10Mg powder at any time. The loss of powder due to the manufacturing of components is compensated by adding a certain amount of virgin powder. In summary, the powder mixture used for the investigation consists of virgin and reused powder. The reused powder, studied in this work, is the result from continuous utilization of the LB-PBF machine over 30 months with a system operation of approx. 2000 h each year. Overall, five samples were collected over the period of 30 months to examine the change in powder quality and hence degradation rate. Table 2 is showing the time frame and annotation for each sample used in this study.

Table 2: The annotation of the samples with respective time in the LB-PBF XLINE 2000R machine.

Sample name	**Time in machine**
Al0	Virgin powder
Al6	6 months
Al10	10 months
Al14	14 months
Al30	30 months

5.1.2 Alloy 718 for LB-PBF

Alloy 718 is from the group of superalloys known for their high strength and oxidation resistance at elevated temperature [67]. This is a Fe-Ni based alloy, which is strengthened by two type of precipitates by ageing heat treatment. Firstly, a disc shaped γ'' (Ni_3Nb) phase is precipitated to increase strength at elevated temperatures, and an additional Ni_3(Al, Ti) cuboid γ' phase is precipitated which further contributes to the precipitation strengthening [68]. The nominal composition of Alloy 718 powder used for the analysis in current study is presented in Table 3. Considering a small fraction of Al and Ti, their importance in the formation of Ni_3(Al, Ti) cuboid γ' precipitates, and their susceptibility for oxidation, it is important to monitor the powder oxidation, spatter oxidation in LB-PBF process, and sublimation in EB-PBF process.

The Alloy 718 powder used was gas atomized and had particles size in the range of 15 µm to 45 µm and was provided by Höganäs AB, Sweden. The particle size distribution (PSD) was verified by laser diffraction using a Mastersizer 3000 (Malvern Panalytical). The results of five measurements provided the following average data: D_{10} = 17.8 ± 0.1 µm, D_{50} = 30.1 ± 0.1 µm, D_{90} =49.5 ± 0.2 µm.

Table 3: Chemical composition of Alloy 718 powder

Element	**wt. %**	**Element**	**wt. %**
Ni	53.95	Co	0.01
Cr	18.28	Mn	0.02
Fe	Bal.	B	0.001
Nb	5.12	Si	0.03
Mo	3.04	Cu	0.04
Ti	1.02	N	90
Al	0.5	O	150
C	0.05	P	<0.01
Ta	<0.01	S	<0.005

5.1.2.1 Processing of Alloy 718 in LB-PBF

This thesis comprises three articles based on Alloy 718 processing in LB-PBF process. There exist some commonalities regarding the equipment and processing parameters, and some differences regarding the build and sampling process among the presented studies. For all the studies, EOS M290 (EOS GmbH) L-PBF machine was used to conduct the study. This system

is equipped with an Yb-fibre laser of 400 W nominal power. The standard EOS parameter for Alloy 718 were used with a 40 µm layer thickness (under the license name: *ALLOY 718_PerformanceM291 2.11*).

For paper II, high-quality argon (Argon 4.6) was used under normal operating condition. To analyze the spatter generation and accumulation in powder bed, capsules were designed to encapsulate powder during the L-PBF process. The containers are fully self-supporting by design and are named after the length and diameter of the beams, e.g., L7D3 (length = 7 mm and diameter = 3 mm). Despite the differences in beam diameter and length, they possessed the same lattice structure, as shown in Figure 11. The three capsules filled with lattice structures, namely Empty, L7D1, L7D3 and L3D1, were placed close to the gas inlet (from where fresh shielding gas enters to cover the process area) on the build platform. The capsules were built on top of a support structure with 2 mm thickness for ease of removal after the build process finished. The caps for the capsules were designed with a thin connection with the body of the container, so that the thin connection can be broken to take the powder samples out for analysis. The powder encapsulated in containers was analyzed using surface and chemical analysis techniques.

An additional aspect of this study was Optical tomography (EOSTATE Exposure OT, supplied by EOS GmbH) to depict on-line spatter formation. The optical tomography was conducted by Dr. Zhuoer Chen and details can be found in the appended paper II.

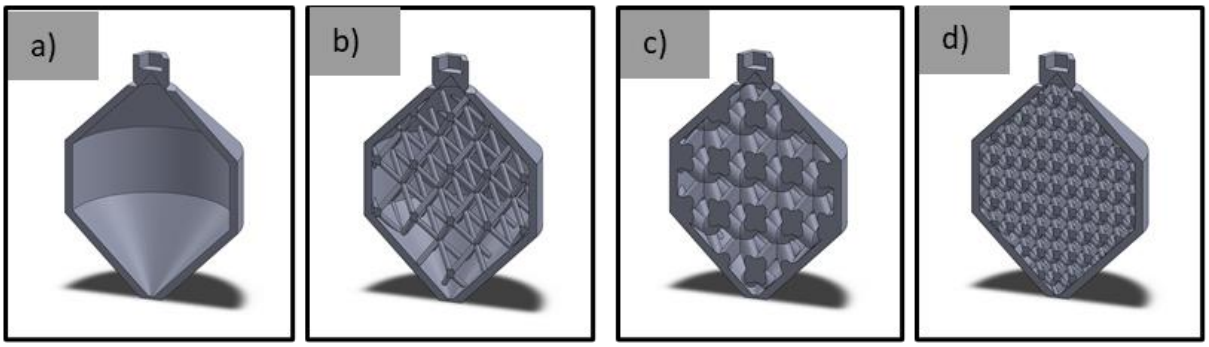

Figure 11: The design illustration of containers with varying dimension of lattice structure which contains a) empty, b) L7D1, c) L7D3, and d) L3D1 capsules. Here, L represents the distance between two parallel bars and joining points and d represent the diameter of the bar in mm (Capsule designed by Z. Chen).

Paper III on Alloy 718 was also conducted in controlled high-quality argon (Argon 4.6) with an oxygen content of around 1000 ppm. In this study, large cylinder with some capsules were built with printing time of 21 h. At the end of printing, spatter particles deposited on gas inlet and outlet were carefully collected and further analyzed to understand the oxidation behavior of Alloy 718 spatters.

In paper IV, high-purity technical Ar (*Argon 5.0* with maximum 10 ppm oxygen) was used as the process gas. An external oxygen monitoring system was connected to the L-PBF machine: the ADDvance®O2 precision (Linde GmbH). During the operation of the ADDvance®O2 precision (Linde GmbH) system, the holding gas flow for the machine, typically present to limit leaks, was manually shut off to stabilize the residual oxygen level. This system enables control of the residual oxygen in the chamber by adjusting the high-purity gas flow within the recirculation system. It measures and controls the purity using an electrochemical cell. The system was used in that work to repeat the same printing cycle under a controlled oxygen

content in the build chamber, with an accuracy of 10 ppm measured with an electrochemical cell, to a minimal level of 20 ppm as well as 400, 600, 800, and 1,000 ppm of residual O_2. During L-PBF processing, a typical deposit on the gas inlet in the build chamber is formed by spatters traveling against the gas flow (toward the gas inlet). These deposits were carefully collected for analysis after each printing cycle, with different oxygen levels in the investigated processing gas.

5.1.3 Alloy 718 for EB-PBF

The material processed for this study was commercially pre-alloyed Alloy 718 powder produced by plasma atomization of wire in an argon atmosphere. The composition of Alloy 718 used in this study is given in Table 4. The powder had particle size distribution of 45 to 105 μm.

Table 4: Chemical composition of the Alloy 718 powder as provided by the powder producer

Elements	Ni	Co	Cr	Mo	Ti	Mn	Nb	Ta	Al	Fe	Si	C
Wt.%	54.1	0.04	19.0	2.99	1.02	0.12	4.97	<0.01	0.52	17.12	0.06	0.03
At.%	53.38	0.04	21.16	1.80	1.23	0.13	3.10	<0.01	1.12	17.75	0.12	0.14

5.1.3.1 EB-PBF processing of Alloy 718

An Arcam EBM A2X machine, located at GE Additive, Gothenburg, Sweden, was used for processing the powder to obtain heat shields. Heat shields are used in EB-PBF machines to protect the surrounding equipment from the effects of temperature and vapor condensation. Heat shields are usually made from 316L stainless steel sheets. The sheets used in the current work had a height of 35 cm and were used for 100h of build time while processing Alloy 718 powder. High vacuum of $\sim 10^{-5}$ mbar was achieved in the chamber before starting the electron beam to remove the residual oxygen from the chamber to avoid powder oxidation. While processing, He gas (grade 5) was introduced, increasing the pressure to $\sim 10^{-3}$ mbar. The powder bed temperature was maintained at 1,000°C to pre-sinter the powder cake to enhance the conductivity and avoid the smoking effect. After a build of 100 h machine time, all four heat shields were carefully removed to avoid contamination of the sheets. These sheets were further used to collect the spatters and condensate for characterization.

5.2 Characterization techniques

5.2.1 Bulk chemical analysis

To analyze the rate of powder degradation over time as well as to estimate the oxygen pick up from virgin powder to spatter particles, bulk chemical analysis of the powder is important. Considering the presence of residual air particularly in LB-PBF process, the analysis of change in O and N during processing of powder is considered vital.

The chemistry of powder was analyzed by combustion gas analysis using LECO ON836 at Höganäs AB. The combustion analysis is based on inert gas fusion (IGF) principle, where the samples are weighed and placed in a graphite crucible. The graphite crucible is moved to furnace where the inert environment is controlled by the flow of He gas. There it is heated to 3000 ^{o}C, and upon melting sample reacts with the walls of crucible. The oxygen present in the sample react with the graphite and form CO and CO_2 gas molecules. The generated gas goes through the detector (non-dispersive infra-red cells) at the gas outlet where the detector using infrared radiation analyze the absorption of CO and CO_2 gas molecules and estimate the

amount of oxygen in the sample. The nitrogen (N_2) releases in the form of N_2 molecules and gets detected using thermal conductivity sensor.

5.2.2 Microscopy

5.2.2.1 Scanning Electron Microscopy (SEM)

The SEM was used for powder morphology, microstructure and fractography analysis using LEO Gemini 1550 (LEO GmbH) SEM equipment, where secondary electrons were collected using In-lens detector. In-Lens detector is commonly used in modern high resolution SEM systems, which detects the secondary electron directly generated from inelastic interaction of the incident electron beam and carry highest spatial resolution information [69]. The powder sample was prepared by mounting the powder particles on the surface of Indium metal plate to avoid any interaction and drift due to carbon tape.

Here, a beam of electron generated by a source (the SEM used in this study has a field emission gun as a source) passes through a series of electromagnetic lenses and incident on the surface of the samples and generates different signals [70]. The intensity of the generated signal can be controlled by the energy of incident electron which can be commonly varied from 3 kV to 30 kV. The incidence beam interaction volume can be several microns and it depends on the beam energy, material type and incidence angle.

SEM is a very dynamic analysis technique which generates a range of signals carrying a diverse amount of information regarding the sample as shown in Figure 12. The generation of these signals is linked with the interaction of electron beam with the electrons in the specimen. There can be primarily two types of interactions: inelastic interaction and elastic interaction. In inelastic interaction, primary electron from incident beam knocks out the secondary electrons by ionizing the atoms in specimen. These electrons normally have a very low energy ($\sim 50\ eV$), hence electrons ejected near the surface can only be detected. Therefore, the detection of secondary electron is very useful to analyze the topology and morphology of the specimen. Contrarily, in elastic interaction, electron bounce back after interacting with the atoms. These electrons are called backscattered electrons (BSE). These electrons can have a bigger interaction volume in the material compared to the secondary electrons as shown in Figure 12. The intensity of BSE varies depending on the atomic number of elements present in the specimen (higher the atomic number means more BSE). Therefore, heavier elements appear brighter in BSE mode as compare to lighter elements, and analysis provide chemical contrast. Finally, ionized atoms in the specimen release excess energy in the process of regaining the original configuration by moving electron from outer shell to inner shells. The generated energy releases in the form of X-rays. The energy of generated X-rays can be used for analyzing the presence of various elements in the specimen, and with the detector principle applied this process is called energy dispersive spectroscopy.

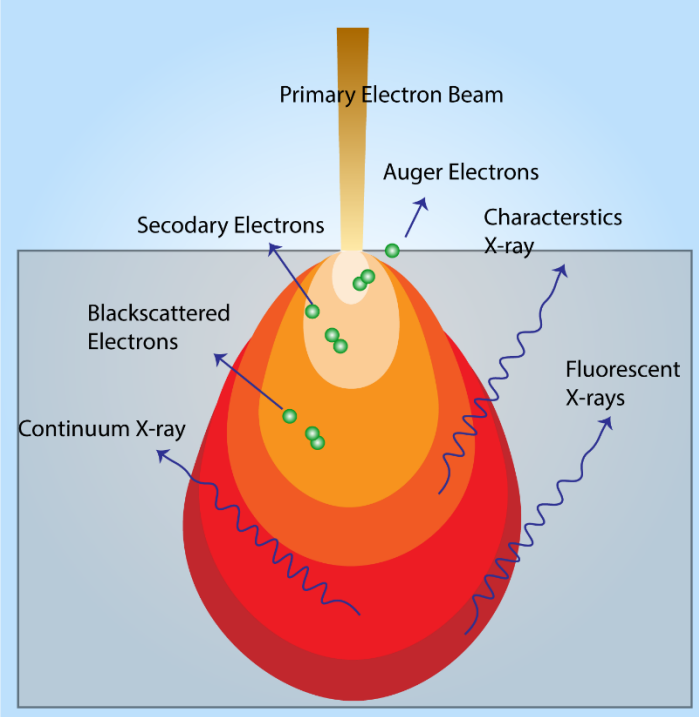

Figure 12: A schematic illustration of electron beam interaction with the specimen and generated signals during scanning electron microscopy analysis.

5.2.2.2 Transmission Electron Microscopy (TEM)

The TEM is a powerful tool to analyze the morphology and chemistry at nano level along with the crystal structure of different phases present in the specimen. For current study, FEI Titan (FEI/Thermo Fisher Scientific, UK) equipped with Silicon Drift (SSD) EDX detector (Oxford Instrument, UK) was used for examining the microstructure, and oxide scale on spatter particles. For oxide morphology and composition analysis, TEM was operated in scanning transmission electron microscopy (STEM) mode at 300 keV and sample was tilted at 15^{o} towards the EDX detector for data acquisition. The sample preparation for TEM sample was done using FEI Versa3D focused ion beam (FIB) milling system, where the sample with typical 100 nm thickness was prepared.

The TEM works on the principle where electron transmits through the material and creates an image. The electron beam can achieve much lower wavelength than light to gain a very high spatial resolution of the sample. In TEM, electron beam is directed to the sample with very high energy (commonly 100-300 KV) focused by a series of electromagnetic lens. The electron passes through the sample and are focused by objective lens and an image in captured on phosphorus screen or through charge-coupled device (CCD) camera.

STEM combines the principle of both SEM and TEM. Like TEM, it requires thin sample for the analysis. A major advantage of STEM over TEM is that it enables the system to use the signals which can be spatially corelated in TEM e.g., secondary electrons, scattered beam electron, characteristic X-rays, and electron energy loss, as shown in Figure 13. Like SEM, STEM scan the finely focused beam in raster pattern over the surface of sample and interaction between incident beam and the specimen generates a series of signals. These signals are correlated with beam position to create a virtual image where the signal level from any point on the specimen is presented by grey level. Scattered beam electrons are detected by high angle

annular dark field (HAADF) detector to create a dark field image. Generated X-rays by incident beam interaction are detected by EDX detector to evaluate the chemistry of the specimen. Lastly, the energy loss during transmission is analyzed by electron energy loss spectroscopy (EELS), which provides the information about surface properties, elemental identity, electronic properties, chemical bonding etc.

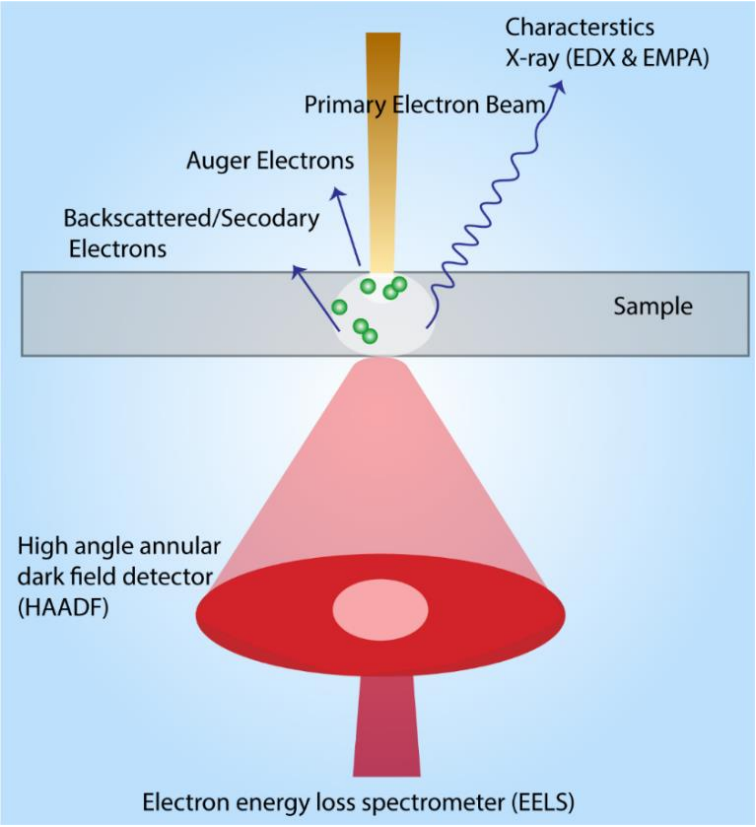

Figure 13: A schematic illustration of electron beam interaction with the specimen and generated signals during scanning transmission electron microscopy analysis.

5.2.3 Surface analysis

Powder degradation is often connected to the chemical changes related to the powder surface. Hence, surface analysis techniques like X-ray photoelectron spectroscopy (XPS) and Auger electron spectroscopy are useful tools to analyze the surface properties. In this study, XPS was mainly used and the details are described in the following section.

5.2.3.1 X-ray Photoelectron Spectroscopy (XPS)

To analyze various aspects (e.g., chemistry, chemical state, thickness of oxide layer, type of oxide, etc.) of specimen surface with exceptional surface resolution (~ 10 nm), XPS is a powerful tool to be used [47,71,72]. As name suggest, X-ray photons are used to generate photoelectron for the analysis. The X-ray photons are generated by striking electron beam on Al/Mg anode, see Figure 14. The generated photons consist of various wavelengths. To get the consistent data, generated X-ray photons are usually passed through a monochromator lens which streamline the photons with single wavelength towards the specimen. Upon interacting with the surface of specimen, the photons excite the electrons from the atoms near the surface. These photoelectrons exit the surface and are collected by an energy analyzer to scan the electron energy scale and then finally to capture the signal by a detector.

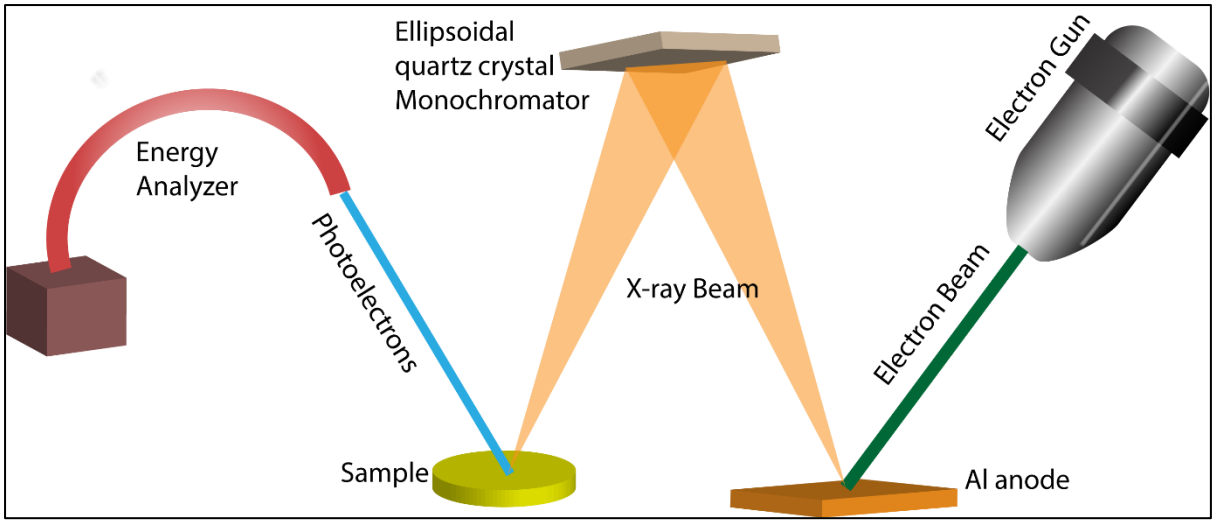

Figure 14: A schematic illustration of XPS system.

The working principle for the analysis of photoelectrons and evaluation of the elemental composition is rather simple. It is usually determined from binding energy (E_b) of detected electrons, which can be derived by subtracting the recorded kinetic energy (E_k) of detected photoelectrons and work-function (W) from the energy of incident X-ray photons ($h\upsilon$) [73]. The work-function is the compensation of energy dissipation of electron from exit to the detection. This all can be represented by following equation:

$$E_b = h\upsilon - E_k - W$$

There are mainly two ways to obtain the data: survey spectra and narrow spectra. Survey spectra is run over a large binding energy range (typically 0-1416 eV) when using Al Kα to detect all the elements present in the surface of specimen. Moreover, narrow scan spectra are used for detailed analysis of any individual element by narrowing the range of binding energy ranger and thus also the energy resolution, for example for detailed analysis of oxygen, O1s spectra with binding energy range 525-538 eV can be used. An additional advantage of XPS is depth profiling where the top surface of the specimen can be ion etched using ionized inert gas beam scanned over the sample surface and the variation in chemical composition and chemical state with depth can be profiled. For this purpose, ion etching at the surface of the sample is performed. A particular strength of XPS is the analysis of chemical state using the high-resolution narrow scan, whereby the fact that core electrons in principle become stronger or weak bound to the nucleus depending if it is a cation or anion state of the element analyzed.

In this thesis, XPS analysis is conducted by using PHI 5500 (Physical Electronics, MN, USA) equipped with monochromator Al Kα source. To avoid any damage on the surface of the powder, the powder was mounted on indium plate (In) for sample preparation. To maximize the statistical authenticity of the data, the analysis area was usually 300 µm × 300 µm. The commonly used pass energies for survey spectra and narrow spectra were 224 eV and 26 eV, respectively. For depth profiling, Ar^+ ion etching was conducted. The etch rate was calibrated on Ta_2O_5 foil and all the depths mentioned in the data are as per that standard. All the data analysis was done using MultiPak 9.7.0.1 software provided by PHI.

6 Results & Discussion

This chapter focuses on the research findings and provides a brief synopsis of the appended papers to this thesis. The whole work is divided mainly in three research questions. First couple of questions are related to the LB-PBF process and the third research question is concerned with EB-PBF process. Appended papers I-V are focused on the discussion regarding the first two research questions. However, the work related to the third research question is still in progress and only sublimation aspect of EB-PBF process is presented in this study.

6.1 RQ1: What is the dominant powder degradation mechanism in LB-PBF process?

To evaluate the dominant powder degradation mechanism, AlSi10Mg was processed for 5000 h of machine time. A careful bulk oxygen and surface analysis showed that spatter accumulation is the dominant powder degradation mechanism. The quantity of spatter particles accumulated in reused powder reached up to 3 % in 30 months reused powder. Surface analysis of spatter particle by TEM showed the formation of a thick (~75-125 nm) oxide layer on the particle surface. The effect of powder degradation on the quality of fabricated parts was also evaluated. The results showed an increase in porosity and decrease in strength with powder reuse. Summary of paper I and II discuss the findings related to RQ1 and are presented below.

6.2 RQ2: What is the correlation between alloy composition and conditions during LB-PBF processing on spatter formation and properties?

A comparison of AlSi10Mg and Alloy 718 powders was done to determine the correlation of alloy composition with nature of developed surface oxide. The oxide formation on AlSi10Mg was rather uniform covering the whole surface of spatter particle. Contrarily, spatter of Alloy 718 showed inhomogeneous oxide particulate and patches formation. Additionally, the effect of geometry on spatter formation was analyzed by changing the component design to vary the surface-to-volume ratio. The results showed that an increase in surface-to-volume ratio and large overhang structures generate higher number of spatters. Finally, the attention was brought towards reducing the extent of oxidation of these spatter particles by varying the residual oxygen content in the build chamber. The aim was to investigate possible correlation between processing atmosphere purity and spatter oxidation. The results showed a decrease in oxidation with decrease in residual oxygen content in the chamber. The summary of paper I, III, IV and V discusses the findings related to RQ2.

6.3 RQ3: What is the dominant powder degradation mechanism in EB-PBF process?

The processing condition in EB-PBF process are dynamically different from LB-PBF process. The EB-PBF process works on a significantly higher temperature and higher vacuum level. Powder degradation of Alloy 718 powder is thoroughly studied in our group by Gruber et al. [7]. His study suggested that powder oxidation is one of the main governing mechanism of oxidation in EB-PBF. However, as was clearly shown in case of LB-PBF, spatter formation is the essential mechanism of powder degradation and there is a lack of literature discussing the properties of spatter and its characteristic in the context of EB-PBF. In addition, as this process is performed in high vacuum and at elevated temperatures, effect of the sublimation of elements during EB-PBF processing of Alloy 718 on powder properties is still not clear. The appended paper VI presents the results obtained while focusing on these aspects by analyzing the retrieved heat shields.

6.4 Summary of appended papers

Paper I

This work has been conducted in collaboration with a research group (Neue Materialien Fürth GmbH) at Friedrich-Alexander Universität Erlangen-Nürnberg, Germany. The research is mainly focused on AlSi10Mg alloy powder, which was processed in a controlled environment of LB-PBF machine. It was interesting to evaluate a powder which was systematically used over the period of 30 months with a complete history of reusability. The left-over powder was sieved after each build in inert atmosphere to maintain the powder size distribution, and the used powder was cyclically compensated with addition of virgin powder to the powder storage of the machine.

A comparison of SEM micrographs between virgin powder (Al0) and 30 months used powder (Al30) did not show a distinguishable difference in the shape and size distribution of powders. However, the presence of some spherically shaped bright particles was noticed only in the case of the reused powder, see Figure 15. The morphological analysis at higher magnification shows that the surface texture of these particles was drastically different from the rest of the powder. By image analysis and statistical calculation of samples, it was found that the number fraction of these particles was increasing in reused powder proportional to the reusability time. As such particles were not present in virgin powder, it was proposed that these are possibly the spatter particles formed by ejecta from melt pool. During the transformation of these particles from melt to solid state, these particles underwent oxidation. This was the reason of difference in surface morphology and brighter contrast during SEM analysis.

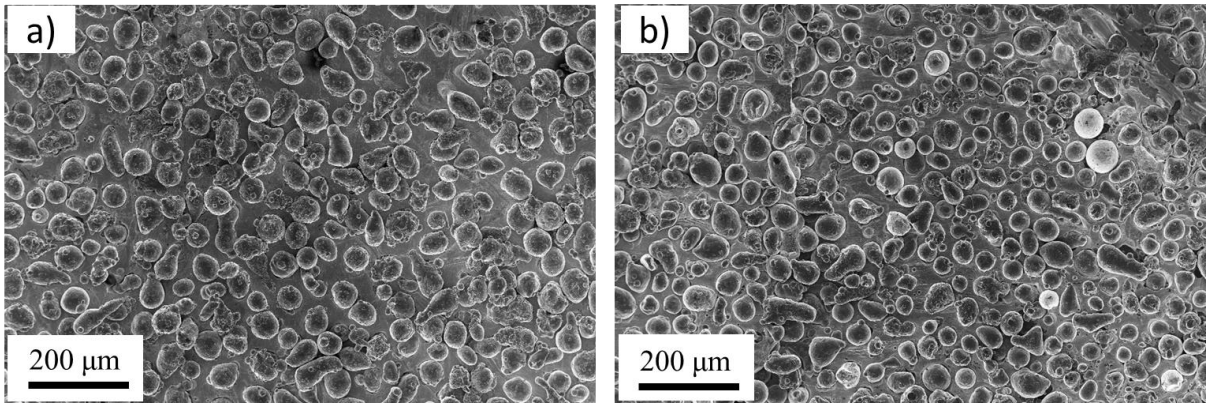

Figure 15: A comparison of AlSi10Mg powder morphology of a) virgin powder with b) 30 months used powder.

Advanced microscopy (TEM) and surface analysis (XPS) techniques were employed to analyze the chemistry of these particles. The TEM analysis revealed that the granular texture on the surface of spatter particles was mainly due to the presence of Al-based oxides along with Mg-based oxide. The thickness of the oxide layer varied between ~75 and 125 nm. Furthermore, the XPS analysis confirmed the presence of Al-based oxide in combination with a $MgAl_2O_4$ type spinel formation, see Figure 16. The oxide layer thickness analysis of the overall powder revealed that the oxide layer thickness increased from 4 nm in virgin powder to around 38 nm in average in 30 months reused powder. A noticeable aspect here is that the oxide layer thickness of overall powder didn't increased much. Therefore, the observed oxide layer thickness in reused was an average oxide layer thickness strongly influenced by thick oxide layer on the surface of spatter particles.

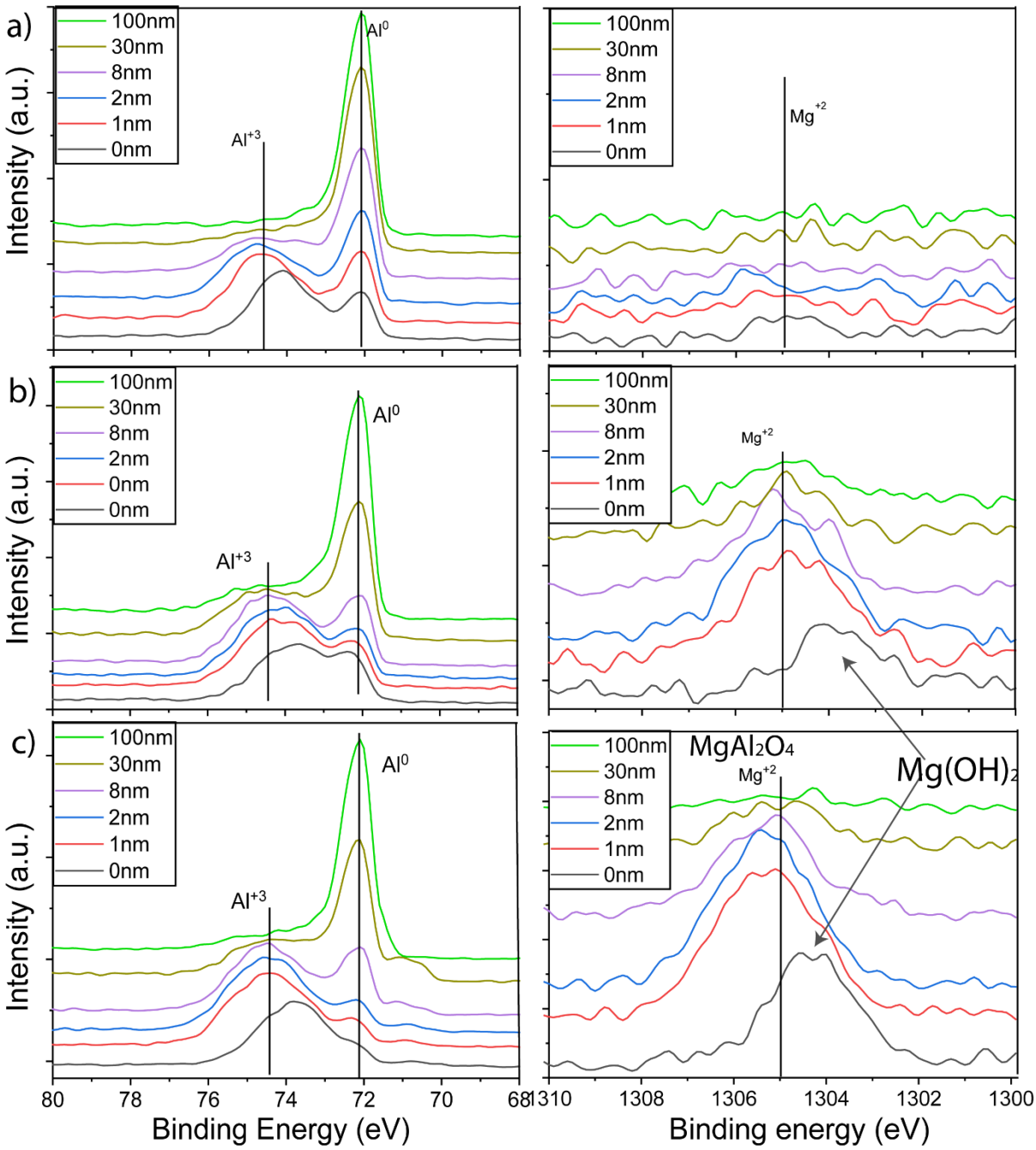

Figure 16: A comparison of depth profile of XPS narrow spectra of Al2p, Mg1s, and O1s from a) Al0 (virgin), b) Al10 (10 months used powder), and c) Al30 (30 months used powder).

Paper II

In this paper the effect of powder degradation, observed in previous study during powder reuse for over 30 months, on microstructure and mechanical behavior was evaluated. The results showed an increase in porosity from <1% to 3% and decrease in strength of ~13%. Firstly, the research efforts were focused on finding the reason for increase in porosity. To evaluate this, the role and amount of hydrogen was closely monitored in components produced from fresh and reused powder. Indeed, H_2 diffusion and segregation on defect sites followed by creation of porosity is a commonly known phenomenon. However, the comparison of hydrogen content in sample produced from fresh (Al0) and the most reused powder (Al30) showed that the

amount of hydrogen was similar in both cases (of ~20 ppm). Hence, hydrogen alone was not responsible for the noted increase in porosity.

Furthermore, the analysis of the fracture surfaces showed a clear difference between samples produced using virgin and recycled powders. First, transgranular dimple ductile fracture was identified as a common micro-failure mechanism in both cases as evidenced by the presence of fine dimples, see Figure 17. In addition, the presence of large pores is evident in both cases, with slightly higher fraction of these defects in case of sample produced from the reused powder. The most important difference between the samples can be seen at higher magnification, see Figure 17 and Figure 18, where significant presence of the oxide residues inside the pores can be seen in case of the reused powder, but not for the virgin powder. This emphasizes the role of the presence of surface oxide phases in the processed powder in the defect formation during LB-PBF. In addition, the presence of thick and extensive oxide inclusions, extending on dozens of micrometers, were observed on the fracture surface of the samples produced from the reused powder, see Figure 18c. Presence of such inclusions on fracture surface, in connection with areas of poor cohesion between the surrounding matrix, explains the measured difference in mechanical properties between the two materials. Hence, the presence of the oxide inclusions in the as-built material from the reused powder has a double impact on the mechanical properties: 1) extensive inclusions, creating weak interfaces in the material and impacting mechanical properties, where even larger impact on dynamic properties can be expected; 2) presence of such interfaces facilitates hydrogen pore formation as well as micro-porosity.

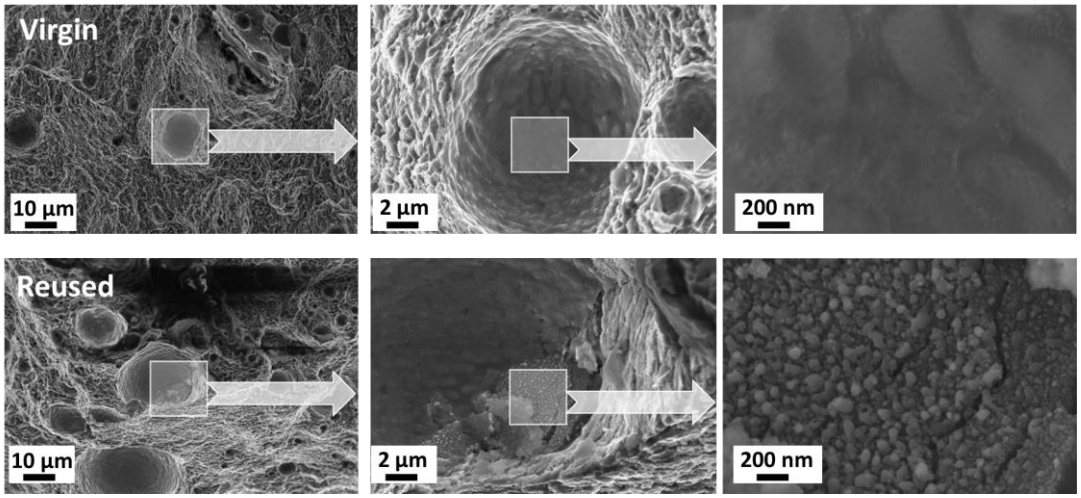

Figure 17: Fracture surface of the samples produced from virgin powder (top) and reused powder (bottom), showing presence of oxide phases in the pores in case of reused sample.

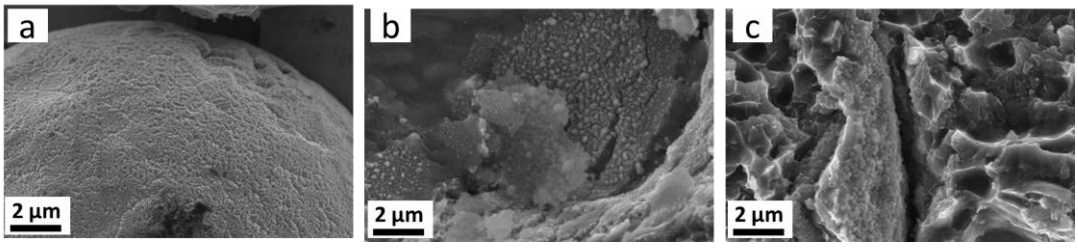

Figure 18: SEM micrographs of the oxidized surface of the AlSi10Mg spatter particle in the reused for 30 months powder a) and appearance of the oxide inclusions in the pore b) and as extensive inclusion c) on the fracture surface of the component produced from this reused powder.

To conclude, the findings of these first two studies suggest that powder oxidation during LB-PBF processing and powder handling is not the dominant powder degradation mechanism. Instead, spatter formation and accumulation in the powder bed is the main factor influencing powder degradation in LB-PBF process, which can result in increasing porosity and decreasing tensile strength of fabricated parts.

To further investigate these findings, a simulated experiment was conducted for Alloy 718 to analyze the effect of product geometry on spatter generation as well as to evaluate the heat effect and effect of spatter accumulation on powder degradation rate. Paper III details the findings of this analysis, which is briefly summarized in the following paragraphs.

Paper III

For this simulated study, special capsules were designed with varying lattice geometry. There were mainly four capsules including empty (E), L7D1, L7D3, and L3D1. Here, L represents the length, and D designates the diameter of lattice struts (both in millimeters). These lattice structures in capsules were designed in order to vary the surface to volume ratio, as well as the amount of specific heat in the capsules. The in-situ optical tomography (OT) was used to trace heat and by-products signals from the scanned area during fabrication.

The OT analysis suggested that the capsules with the lattice dimensions of L7D3 and L3D1 showed higher amount of grey value (GV) signals compared to the empty container, see Figure 19. This was due to denser and thicker lattice geometries in these capsules. Larger GV signals suggest that the geometry with large surface-to-volume ratio (L3D1) and large area of overhangs have higher tendency to generate by-products. The SEM analysis of powder samples obtained from the capsules confirmed that the samples from L7D3 and L3D1 has higher number of spatters and correlates well with the findings of OT data analysis.

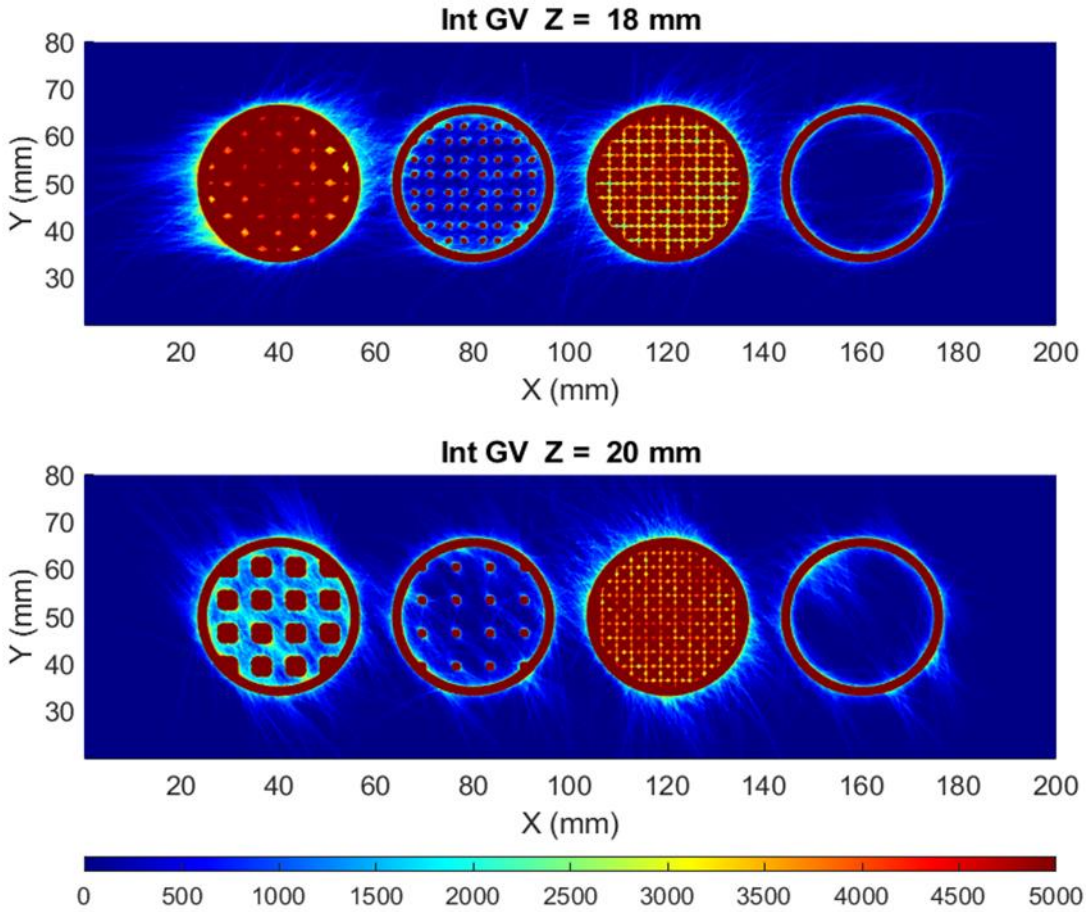

Figure 19:OT images at three different build heights. The color scale for GVs is adjusted to show the presence of process by-products such as spatter particles (Analysis done by Z. Chen).

For correlation of OT data with powder chemistry and surface chemical composition, oxygen content analysis and XPS analysis of the obtained samples was conducted. The oxygen content analysis showed no substantial change in oxygen content from the virgin powder to the empty and L7D1 capsules. However, a 22 % and 49 % increase compared to virgin powder was observed in the samples obtained from L3D1 and L7D3 capsules respectively. This increase was driven by higher amount of spatter accumulation in these capsules. Similarly, XPS analysis showed that the normalized oxygen content increased in L3D1 and L7D3 capsules at higher etched depth as compared to the virgin powder, which was also influenced by the presence of spatter particles.

To summarize, this study provided a very good relationship between component geometry and by-product generation. The amount of by-product accumulation also provided an insight regarding the degradation of the powder. To pursue this and study the oxidation behavior and nature of oxides on the surface of spatter particles, an additional study was done. Here, the spatter particles generated during the process were collected at the gas outlet and inlet. A comprehensive microstructure and surface analysis was conducted to establish the oxidation behavior of spatter particles. This is presented in the 4th appended paper, and it is briefly discussed in the following section.

Paper IV

This is a dedicated study to analyze the spatter samples carefully collected from the gas inlet and outlet after the built, see Figure 20. This study provides an insight into spatter oxidation mechanism and oxygen pick-up during the processing of Alloy 718. Sampled powder were analyzed using bulk oxygen analysis, SEM analysis, and XPS analysis. Following paragraphs summarize the findings from these analyses.

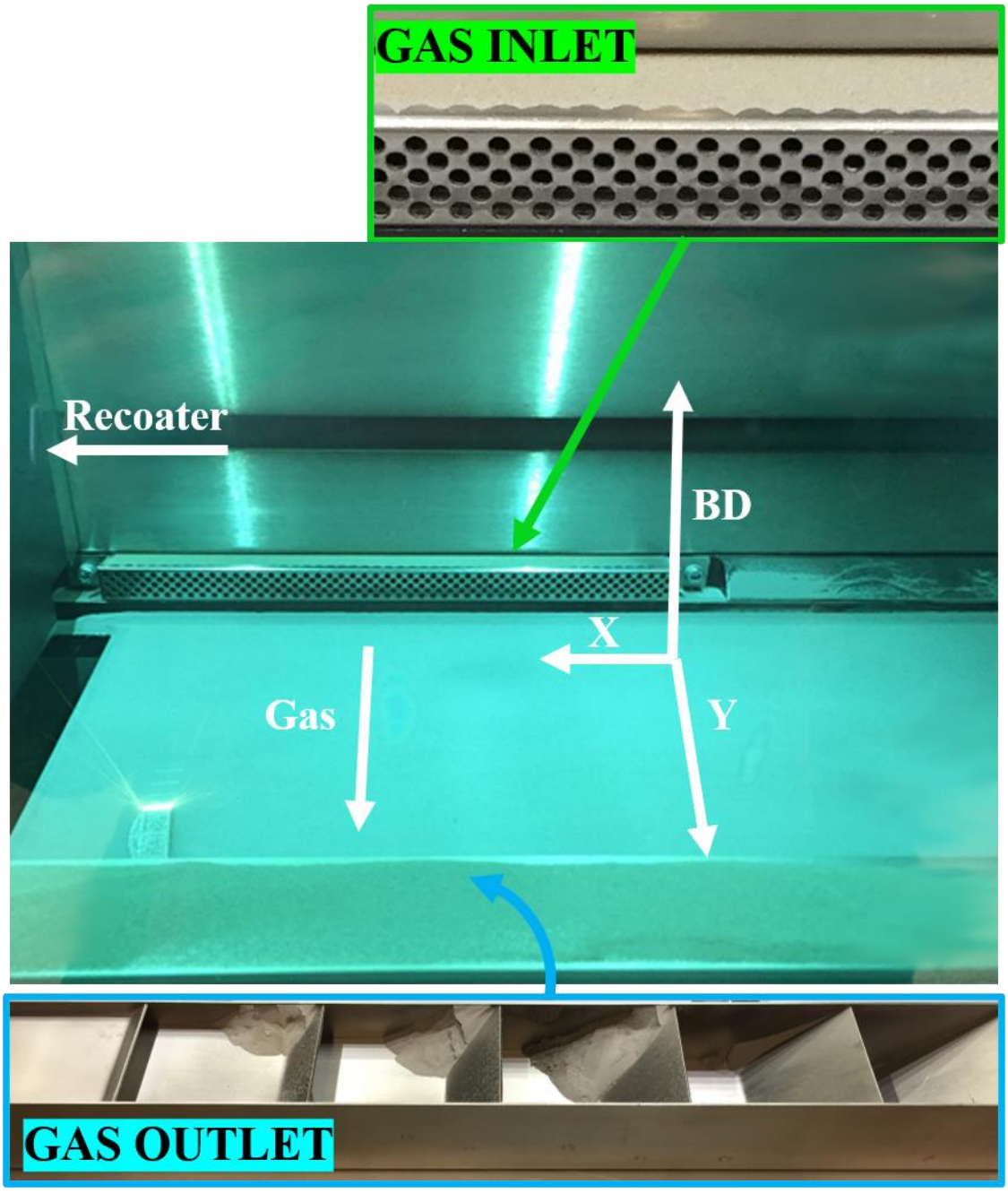

Figure 20: Photograph of the build chamber taken from the window of M290 EOS machine. The inserts show the close-up of the gas inlet and outlet from where samples were collected.

Bulk oxygen analysis by combustion test showed more than a 100 % increase in oxygen content of spatter particles collected from both inlet and outlet spatter particles compared to the virgin composition. The morphology analysis by SEM shows that the spatter particles collected both on the gas inlet and outlet have thick oxide particulates and patches on their surface. The

morphology analysis suggests that the spatter oxidation mechanism is drastically different in Alloy 718 compared to AlSi10Mg alloy for which the whole particle surface was uniformly oxidized. To characterize the type, nature, and thickness of surface oxides, XPS analysis was performed. The analysis by XPS narrow spectra suggests that the appeared oxide particulates and patches are dominantly Al- and Cr-based oxides, which is connected to the higher susceptibility of these elements for oxidation. Normalized oxygen content analysis showed a substantial increase in oxygen content at larger etch depths as compared to the virgin sample, thereby indicating a higher oxide layer thickness on these spatters compared to virgin powder.

To further evaluate the thermal history of spatter powder compared to virgin powder, a detailed microstructural analysis was performed. This analysis was helpful to differentiate the entrained spatter particles from melt ejecta (entrained particles are only affected by heat and were not fully molten). The analysis showed the presence of both primary and secondary dendrites in entrained particles, which was similar to virgin powder. However, the melt ejecta showed only primary dendrites and no secondary dendrites. This difference is linked to the difference in cooling rate both in atomizer and LB-PBF build chamber. Solidification rate calculations showed that the cooling rate of melt ejecta in LB-PBF system was one order of magnitude higher than what experienced during atomization. Furthermore, the results highlighted that most of the spatter particles collected at the gas inlet and outlet were entrained particles with partially heated/melted surface. This partial heating and/or melting of entrained particles resulted in the observed oxidation in the form of patches and particulates. In contrast, the complete surface oxidation of AlSi10Mg spatter is probably connected to the lower melting point of the alloy, for which even more of the entrained spatter particles were melted and solidified before depositing on the powder bed.

From paper III and Paper IV, it is evident that the spatter generation and oxidation during LB-PBF is unavoidable. Therefore, there was a need to develop approaches to reduce the extent of oxidation on the generated spatter particles. Next appended paper presents a way to reduce the oxidation by reducing the residual oxygen content in the build chamber atmosphere.

Paper V

To evaluate the effect of the residual oxygen content in the process chamber on extent of spatter oxidation, the oxygen partial pressure carefully monitored by an external system, the ADDvance®O2 precision (Linde GmbH), was varied from 20 ppm to 1000 ppm. The samples were collected from the gas inlet, which consist mostly of entrained spatter particles. Figure 21 displays the deposited spatters on the gas inlet, where a clear discoloration of powder can be seen in connection with the increase in oxygen content from grey to brown appearance. This discoloration is linked with the extent of spatter oxidation, which is increasing with the increase in residual oxygen content in the chamber.

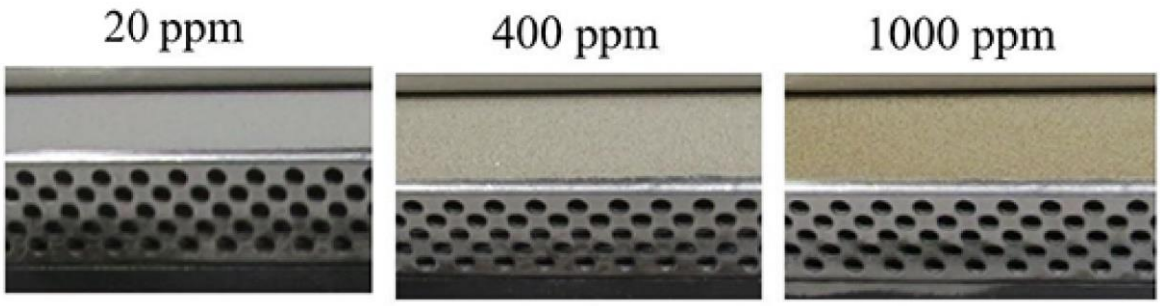

Figure 21: Deposited Alloy 718 spatter on the gas outlet, where a distinguishable discoloration with increase in residual oxygen content in the process atmosphere can be noticed.

The bulk oxygen analysis showed a dependency of oxygen pick-up on the residual oxygen content. From the virgin sample to the sample collected at 20 ppm oxygen level, an increase of ~30 % in oxygen content was observed. However, the increase was more drastic for higher O_2 partial pressure, and above 300 % increase in oxygen content was measured for the sample obtained under 1000 ppm residual oxygen level – the standard operating level of most LB-PBF machines. This change can also be clearly seen by analyzing the morphology of the collected samples, as shown in Figure 22. At lower oxygen content, thin oxide patches formation can be observed. However, with the increase in residual oxygen content, the oxide patches grow thicker, and oxide particulate formation was also prevalent.

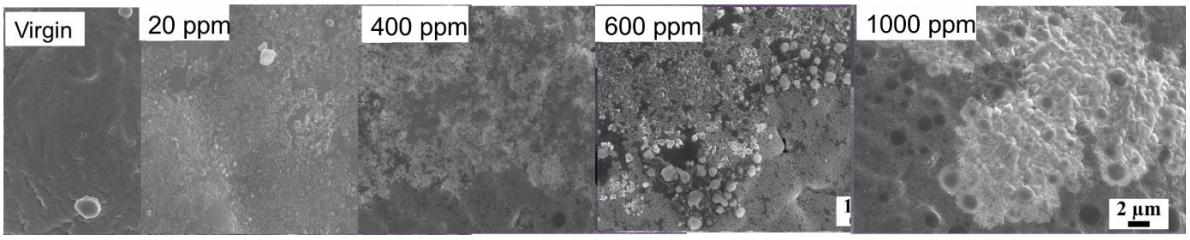

Figure 22: A comparison of morphology of virgin powder with spatter particles collected at 20 ppm, 400 ppm, 600 ppm, and 1000 ppm.

The XPS survey spectra and narrow spectra analysis showed that the surface was dominantly oxidized by Al- and Cr-based oxides. By fitting of the O1s and $Cr2p_{3/2}$ spectra, it was observed that Al was a more dominant oxidizing element at lower oxygen level as compared to Cr. The contribution of Cr to the oxide layer at 20 ppm O_2 was minimal as compared to that of Al. However, with increasing residual oxygen, Cr also became a dominantly oxidized element alongside Al. This was further evaluated by Thermo-calc and Dictra calculations, which showed that it is possible for Al to oxidize at very scarce amount of oxygen compare to Cr. The normalized oxygen content estimation shows a substantial increase in oxygen content at larger depth with increase in residual oxygen content, see Figure 23a. The thickness of oxide patches and particulates also significantly increased from 20 ppm (~15 nm) to 1000 ppm O_2 (~75 nm), see Figure 23b. The oxide layer thickness from $Cr2p_{3/2}$ narrow spectra is compared to the overall oxide layer thickness measured through O1s. This indicates thicker Al-based oxide patches and particulate formation compared to Cr.

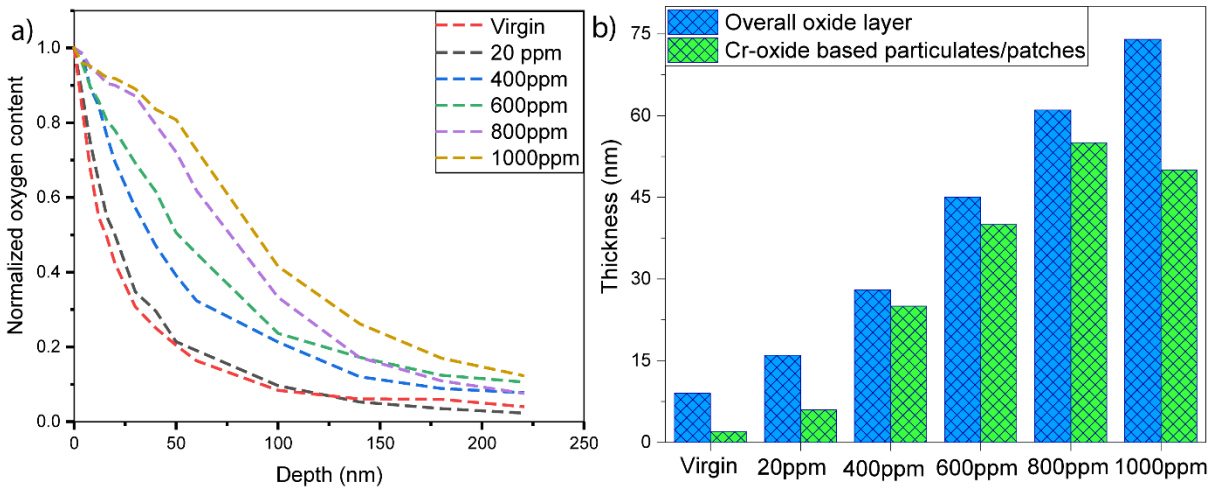

Figure 23: a) A comparison of normalized oxygen content calculated based on XPS depth profile, and b) Calculated Cr-based oxide particulates/patches thickness and overall oxide layer thickness of all samples. Cr-oxide layer thickness was calculated from $Cr2p_{3/2}^{met}$ spectra, and overall oxide layer thickness was calculated through O1s spectra.

A detailed thermodynamic analysis calculating the driving forces, diffusion, and reactivity of all constituents in Alloy 718 was also conducted and presented in paper V. The calculations confirmed the preferential oxidation of Al at lower residual oxygen levels, and the enrichment in Cr upon increasing O_2 partial pressure.

Paper VI

To evaluate the sublimation occurring during the EB-PBF process of Alloy 718, heat shields which cover the build area and protect the machine from heat effect and vapors, were studied. Heat shields get covered with the sublimated vapors in the form of both condensates and spatters which land on the surface of heat shield. Figure 24 illustrates the distribution of spatters and condensates on the surface of heat shield. Both the spatters and condensates were preferentially deposited towards the bottom of the heat shield. The thickness of condensate reached a thickness of >50 µm at the bottom, while it was only 5 µm at the top. Spatter particle analysis shows that the spatter surface was also covered with the condensate vapors, and the thickness of deposited condensate on spatter surface varied depending on the time on heat shield.

The chemical analysis of spatter particles covered with condensates showed an increase of about 17 times in oxygen content compared to the virgin powder. The EDS analysis of the condensate on spatter surface showed that the condensates are dominantly consisting of Cr-based oxide. Hence, it is concluded that Cr is one of the major sublimating element in case of Alloy 718. Considering the importance of Cr for corrosion and high temperature oxidation resistance for Alloy 718 components, monitoring of the Cr content both in the leftover powder and fabricated parts is vital. To conclude, this study suggests that the sublimation can be a potential degradation mechanism for powders as well as fabricated parts in EB-PBF process.

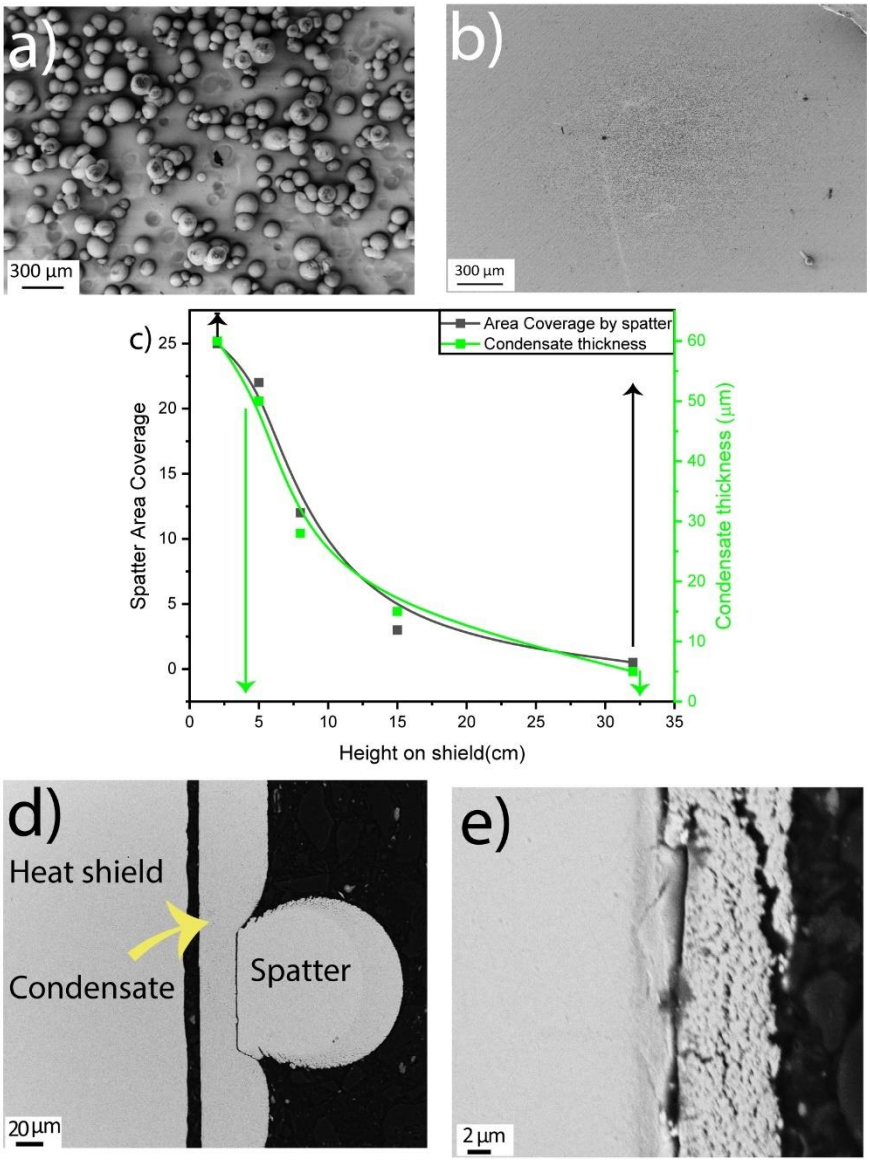

Figure 24: The top micrographs show an area covered by spatters from the a) bottom (2 cm) and b) top (~32 cm) of the heat shield (distances from the bottom of the heat shield). The center plot c) shows the variation in area coverage by spatter particles and condensate thickness with height on the heat shield. The bottom micrographs show the condensate thickness d) at the bottom (2 cm) and e) top (32 cm) of the heat shield.

7 Conclusions

Multiple conclusions can be drawn from the findings of this work. The conclusions are divided based on research questions:

RQ1: What is the dominant powder degradation mechanism in LB-PBF process?

- The analysis of AlSi10Mg powder showed that spatters accumulation can be a potentially dominant powder degradation mechanism as the analysis showed that accumulated spatters in the powder after 30 months of reuse reached to a number fraction of above 3 %. Accumulated spatter amount increased the average oxide layer thickness from 4 nm to 38 nm after 30 months of reuse. This degradation of powder had a detrimental effect on the properties of fabricated parts. The parts fabricated from reused powder showed an increase in porosity from <1% to 3%, and ~13% decrease in tensile strength.

RQ2: What is the correlation between alloy composition and conditions during LB-PBF processing on spatter formation and properties?

- The geometry effect on spatter generation in Alloy 718 showed that the area to volume ratio and overhang structures can substantially contribute to increase in the spatter generation. The optical tomography analysis show that the capsules with higher area to volume ratio (L3D1) and larger overhang structure (L7D3) showed higher heat signals. Also, these capsules showed higher oxygen pick up (L3D1 showed 22 % and L7D3 showed 49 % increase compare to virgin) which reaffirms the presence of higher amount spatters.
- A detailed investigation of Alloy 718 spatter samples collected from gas inlet and outlet showed that the bulk oxygen content increased to ~600 ppm spatter particles as compare to virgin samples (~267 ppm). The surface of these particles was partially oxidized due to heating/partial melting of such particles. Particle surface was covered with Al and Cr based oxide patches and particulates.
- Combined analysis of part geometry effect on spatter generation and spatter oxidation assisted in concluding that spatters are unavoidable by-products in LB-PBF process. The way to minimize their impact in powder degradation is to control of their extent of oxidation by process atmosphere control. Relationship between residual oxygen content and extent of spatter oxidation showed that the residual oxygen content in chamber directly affects the oxidation of spatters. Reduction of residual oxygen content in the chamber can assist in slowing the rate of powder degradation and increase in the life of leftover powder in LB-PBF process. The analysis showed that the thickness of oxide patches and particulates significantly decreased from ~75 nm at 1000 ppm O_2 to ~15 nm at 20 ppm.

RQ3: What is the dominant powder degradation mechanism in EB-PBF process?

- The analysis of heat shields, obtained from EBM A2X machine, showed that Cr is a major sublimating element along with Al during processing of Alloy 718. Considering the role of Cr in oxidation and corrosion resistance in Alloy 718 components, the content of Cr and Al should be closely monitored both in fabricated parts, and leftover unconsumed powder.

8 Future Work

In the LB-PBF part of the current study, by using intensive surface analysis techniques supported by thermodynamic calculations, it has been established that spatter particles oxidation and accumulation is the major powder degradation mechanism. This knowledge provides a basis to determine the correlation between spatter formation and properties with respect to the used materials and gas atmosphere. Firstly, the spatter oxidation behavior of various materials including other alloys systems, as e.g. TiAl6V4, iron-based alloys as stainless steel 316L, Ni-base superalloys and copper alloys can be studied using a similar analysis methodology. It will be interesting to compare the variations in oxidation behavior of spatters with changes in alloy type. Moreover, as appended paper V has shown the effect of atmospheric purity on spatter oxidation, the impact of atmospheric gas (argon, helium, nitrogen, etc.) on the nature and type of oxides formed on spatter particles surface also requires further investigation.

Paper 2 determined the effect of reused powder on the properties of fabricated parts. To determine the impact of spatter oxidation and accumulation on the properties of fabricated parts, there is a need to systematically study the properties of parts fabricated through reused powder. The defects caused by spatter accumulation and powder oxidation are usually lack fusion defects and nonmetallic inclusions. Such defects do not substantially affect static properties (tensile properties, etc.). Therefore, there is a need to evaluate the fatigue properties of such parts for a better understanding of degradation.

The EB-PBF part in this thesis is not comprehensively studied yet. There are various aspects that require further understanding, particularly regarding Ti alloys (TiAl6V4 and TiAl). Usually, Ti alloys pick up oxygen both in oxides and in dissolved form. Comprehensive surface analysis of TiAl6V4 and TiAl can provide useful information regarding the nature of oxygen pickup in Ti alloys during the EB-PBF process. This study can be combined with the sublimation behavior analysis of different alloys, in particular TiAl6V4 alloy. Lastly, it can be interesting to study the effect of powder oxidation and sublimation on the properties of fabricated parts.

9 Acknowledgement

I would like to thank my supervisor Prof. Eduard Hryha and examiner Prof. Lars Nyborg for providing me this opportunity to explore an interesting dimension of additive manufacturing. Additionally, I would like to express my gratitude to Prof. Eduard Hryha for his guidance and untiring support.

A special thanks to Dr. Camille Pauzon for mentorship, collaboration, and so many corrections in manuscripts. Also, I appreciate the support and contribution of other co-authors particularly Tobias Fiegl from FAU Erlangen, Germany, and Dr. Z. Chen. Furthermore, I would like to thank Andreas Markström for his support in Thermo-Calc-related calculations.

Dr, Eric Tam deserves special thanks for teaching me the XPS technique, tolerating my mistakes, and answering my unending streak of questions about it. Additionally, I would also express my appreciation for Dr. Yiming Yao, Dr. Yu Cao, Engr. Roger Sagdahl, and Jessica Twedmark for their support during this time.

Thanks to all the colleagues in the Department of Industrial and Materials Science who made me feel at home. Special thanks to my colleagues in AM/PM group including Bala, William, Dmitri, Anok, Bharat, William, Rasmus, Swathi, Alberto, Claudia, Fiona, and my officemates Laura and Philip for sharing ideas and discussions. A shout out to Dmitri Riabov for making bulk chemical analysis possible from Höganäs.

My friends outside the workplace in Gothenburg, Awais, Imran, Zazy, Rizwan, Muti also deserve thanks for being there during hard times caused by COVID19.

Lastly, I would like to acknowledge my family for their support and patience.

10 References

[1] S. Brischetto, P. Maggiore, C.G. Ferro, Additive Manufacturing Technologies and Applications, MDPI, 2018. https://doi.org/10.3390/books978-3-03842-549-6.

[2] A. Rashid, Additive Manufacturing Technologies, 2019. https://doi.org/10.1007/978-3-642-35950-7_16866-1.

[3] V. Seyda, N. Kaufmann, C. Emmelmann, Investigation of Aging Processes of Ti-6Al-4 v Powder Material in Laser Melting, in: Phys. Procedia, 2012: pp. 425–431. https://doi.org/10.1016/j.phpro.2012.10.057.

[4] J.H. Martin, B.D. Yahata, J.M. Hundley, J.A. Mayer, T.A. Schaedler, T.M. Pollock, 3D printing of high-strength aluminium alloys, Nature. 549 (2017) 365–369. https://doi.org/10.1038/nature23894.

[5] L. Cordova, T. Bor, M. de Smit, M. Campos, T. Tinga, Measuring the spreadability of pre-treated and moisturized powders for laser powder bed fusion, Addit. Manuf. 32 (2020) 101082. https://doi.org/10.1016/j.addma.2020.101082.

[6] C. Rock, C. Ledford, M. Garcia-Avila, H. West, V.M. Miller, M. Pankow, R. Dehoff, T. Horn, The Influence of Powder Reuse on the Properties of Nickel Super Alloy ATI 718^{TM} in Laser Powder Bed Fusion Additive Manufacturing, Metall. Mater. Trans. B Process Metall. Mater. Process. Sci. (2021). https://doi.org/10.1007/s11663-020-02040-2.

[7] H. Gruber, M. Henriksson, E. Hryha, L. Nyborg, Effect of Powder Recycling in Electron Beam Melting on the Surface Chemistry of Alloy 718 Powder, Metall. Mater. Trans. A. 50 (2019) 4410–4422. https://doi.org/10.1007/s11661-019-05333-7.

[8] C. Pauzon, A. Raza, E. Hryha, P. Forêt, Oxygen balance during laser powder bed fusion of Alloy 718, Mater. Des. 201 (2021). https://doi.org/10.1016/j.matdes.2021.109511.

[9] C. Pauzon, E. Hryha, P. Forêt, L. Nyborg, Effect of argon and nitrogen atmospheres on the properties of stainless steel 316 L parts produced by laser-powder bed fusion, Mater. Des. 179 (2019) 107873. https://doi.org/10.1016/j.matdes.2019.107873.

[10] A. Raza, T. Fiegl, I. Hanif, A. Markström, M. Franke, C. Körner, E. Hryha, Degradation of AlSi10Mg powder during laser based powder bed fusion processing, Mater. Des. 198 (2021) 109358. https://doi.org/10.1016/j.matdes.2020.109358.

[11] A. Montelione, S. Ghods, R. Schur, C. Wisdom, D. Arola, M. Ramulu, Powder Reuse in Electron Beam Melting Additive Manufacturing of Ti6Al4V: Particle Microstructure, Oxygen Content and Mechanical Properties, Addit. Manuf. 35 (2020) 101216. https://doi.org/10.1016/j.addma.2020.101216.

[12] H. Gruber, C. Luchian, E. Hryha, L. Nyborg, Effect of Powder Recycling on Defect Formation in Electron Beam Melted Alloy 718, Metall. Mater. Trans. A Phys. Metall. Mater. Sci. 51 (2020) 2430–2443. https://doi.org/10.1007/s11661-020-05674-8.

[13] L. Cordova, M. Campos, T. Tinga, Revealing the Effects of Powder Reuse for Selective Laser Melting by Powder Characterization, JOM. 71 (2019) 1062–1072. https://doi.org/10.1007/s11837-018-3305-2.

[14] K. Zumsande, A. Weddeling, E. Hryha, S. Huth, L. Nyborg, S. Weber, N. Krasokha,

W. Theisen, Characterization of the surface of Fe-19Mn-18Cr-C-N during heat treatment in a high vacuum - An XPS study, Mater. Charact. 71 (2012) 66–76. https://doi.org/10.1016/j.matchar.2012.06.002.

[15] M. Simonelli, C. Tuck, N.T. Aboulkhair, I. Maskery, I. Ashcroft, R.D. Wildman, R. Hague, A Study on the Laser Spatter and the Oxidation Reactions During Selective Laser Melting of 316L Stainless Steel, Al-Si10-Mg, and Ti-6Al-4V, Metall. Mater. Trans. A Phys. Metall. Mater. Sci. 46 (2015) 3842–3851. https://doi.org/10.1007/s11661-015-2882-8.

[16] A.N.D. Gasper, B. Szost, X. Wang, D. Johns, S. Sharma, A.T. Clare, I.A. Ashcroft, Spatter and oxide formation in laser powder bed fusion of Inconel 718, Addit. Manuf. 24 (2018) 446–456. https://doi.org/10.1016/j.addma.2018.09.032.

[17] A.N.D. Gasper, D. Hickman, I. Ashcroft, S. Sharma, X. Wang, B. Szost, D. Johns, A.T. Clare, Oxide and spatter powder formation during laser powder bed fusion of Hastelloy X, Powder Technol. 354 (2019) 333–337. https://doi.org/10.1016/j.powtec.2019.06.004.

[18] C. Pauzon, P. Forêt, E. Hryha, T. Arunprasad, Effect of Helium - Argon Mixtures as Laser - Powder Bed Fusion Processing Atmospheres on the Properties of the Built Ti-6Al-4V Parts, WorldPM2018. (2018) 1633–1639.

[19] L.C. Ardila, F. Garciandia, J.B. González-Díaz, P. Álvarez, A. Echeverria, M.M. Petite, R. Deffley, J. Ochoa, Effect of IN718 recycled powder reuse on properties of parts manufactured by means of Selective Laser Melting, in: Phys. Procedia, Elsevier B.V., 2014: pp. 99–107. https://doi.org/10.1016/j.phpro.2014.08.152.

[20] M.J. Heiden, L.A. Deibler, J.M. Rodelas, J.R. Koepke, D.J. Tung, D.J. Saiz, B.H. Jared, Evolution of 316L stainless steel feedstock due to laser powder bed fusion process, Addit. Manuf. 25 (2019) 84–103. https://doi.org/10.1016/j.addma.2018.10.019.

[21] V. Gunenthiram, P. Peyre, M. Schneider, M. Dal, F. Coste, I. Koutiri, R. Fabbro, Experimental analysis of spatter generation and melt-pool behavior during the powder bed laser beam melting process, J. Mater. Process. Technol. 251 (2018) 376–386. https://doi.org/10.1016/j.jmatprotec.2017.08.012.

[22] A. Bin Anwar, Q.C. Pham, Study of the spatter distribution on the powder bed during selective laser melting, Addit. Manuf. 22 (2018) 86–97. https://doi.org/10.1016/j.addma.2018.04.036.

[23] A.T. Sutton, C.S. Kriewall, M.C. Leu, J.W. Newkirk, B. Brown, Characterization of laser spatter and condensate generated during the selective laser melting of 304L stainless steel powder, Addit. Manuf. 31 (2020) 100904. https://doi.org/10.1016/j.addma.2019.100904.

[24] M. Molitch-Hou, Overview of additive manufacturing process, Elsevier Inc., 2018. https://doi.org/10.1007/978-981-10-6591-0_4.

[25] T. Özel, A. Altay, B. Kaftanoglu, R. Leach, N. Senin, A. Donmez, Focus variation measurement and prediction of surface texture parameters using machine learning in laser powder bed fusion, J. Manuf. Sci. Eng. Trans. ASME. 142 (2020). https://doi.org/10.1115/1.4045415.

[26] L.C. Zhang, Y. Liu, S. Li, Y. Hao, Additive Manufacturing of Titanium Alloys by Electron Beam Melting: A Review, Adv. Eng. Mater. 20 (2018) 1–16. https://doi.org/10.1002/adem.201700842.

[27] S. Biamino, A. Penna, U. Ackelid, S. Sabbadini, O. Tassa, P. Fino, M. Pavese, P. Gennaro, C. Badini, Electron beam melting of Ti-48Al-2Cr-2Nb alloy: Microstructure and mechanical properties investigation, Intermetallics. 19 (2011) 776–781. https://doi.org/10.1016/j.intermet.2010.11.017.

[28] E. Hryha, D. Riabov, Metal Powder Production for Additive Manufacturing, Encycl. Mater. Met. Allloys. 3 (2022) 264–271. https://doi.org/10.1016/b978-0-12-819726-4.00089-2.

[29] S.E. Brika, M. Letenneur, C.A. Dion, V. Brailovski, Influence of particle morphology and size distribution on the powder flowability and laser powder bed fusion manufacturability of Ti-6Al-4V alloy, Addit. Manuf. 31 (2020) 100929. https://doi.org/10.1016/j.addma.2019.100929.

[30] J.J. Dunkley, Metal powder atomisation methods for modern manufacturing, Johnson Matthey Technol. Rev. 63 (2019) 226–232. https://doi.org/10.1595/205651319X15583434137356.

[31] C.F. Dixon, Atomizing molten metals-a review, Can. Metall. Q. 12 (1973) 309–321. https://doi.org/10.1179/cmq.1973.12.3.309.

[32] L.V.M. Antony, R.G. Reddy, Processes for production of high-purity metal powders, Jom. 55 (2003) 14–18. https://doi.org/10.1007/s11837-003-0153-4.

[33] D. Riabov, E. Hryha, M. Rashidi, S. Bengtsson, L. Nyborg, Effect of atomization on surface oxide composition in 316L stainless steel powders for additive manufacturing, Surf. Interface Anal. 52 (2020) 694–706. https://doi.org/10.1002/sia.6846.

[34] M. Entezarian, F. Allaire, P. Tsantrizos, R.A.L. Drew, Plasma atomization: A new process for the production of fine, spherical powders, Jom. 48 (1996) 53–55. https://doi.org/10.1007/BF03222969.

[35] A. Strondl, O. Lyckfeldt, H. Brodin, U. Ackelid, Characterization and Control of Powder Properties for Additive Manufacturing, Jom. 67 (2015) 549–554. https://doi.org/10.1007/s11837-015-1304-0.

[36] J.A. Slotwinski, E.J. Garboczi, P.E. Stutzman, C.F. Ferraris, S.S. Watson, M.A. Peltz, Characterization of metal powders used for additive manufacturing, J. Res. Natl. Inst. Stand. Technol. 119 (2014) 460–493. https://doi.org/10.6028/jres.119.018.

[37] A.T. Sutton, C.S. Kriewall, S. Karnati, M.C. Leu, J.W. Newkirk, Characterization of AISI 304L stainless steel powder recycled in the laser powder-bed fusion process, Addit. Manuf. 32 (2020) 100981. https://doi.org/10.1016/j.addma.2019.100981.

[38] H.L. Lukas, S.G. Fries, B. Sundman, Computational thermodynamics: The Calphad method, 2007. https://doi.org/10.1017/CBO9780511804137.

[39] J.O. Andersson, T. Helander, L. Höglund, P. Shi, B. Sundman, Thermo-Calc & DICTRA, computational tools for materials science, Calphad Comput. Coupling Phase Diagrams Thermochem. 26 (2002) 273–312. https://doi.org/10.1016/S0364-5916(02)00037-8.

[40] E. Hryha, R. Shvab, H. Gruber, A. Leicht, L. Nyborg, Surface oxide state on metal powder and its changes during additive manufacturing: An overview, in: Proc. Euro PM 2017 Int. Powder Metall. Congr. Exhib., 2018.

[41] S.K. Manchili, J. Wendel, E. Hryha, L. Nyborg, Analysis of iron oxide reduction kinetics in the nanometric scale using hydrogen, Nanomaterials. 10 (2020) 1–17. https://doi.org/10.3390/nano10071276.

[42] A.N. and I.O. L. Nyborg, Thickness Determination of Oxide Layers on Spherically-shaped Metal Powders by ESCA, 12 (1988) 110–114. https://doi.org/doi: 10.1002/sia.740120209.

[43] I. Olefjord, L. Nyborg, Surface analysis of gas atomized ferritic steel powder, Powder Metall. 28 (1985) 237–243. https://doi.org/10.1179/pom.1985.28.4.237.

[44] E. Hryha, R. Shvab, M. Bram, M. Bitzer, L. Nyborg, Surface chemical state of Ti powders and its alloys: Effect of storage conditions and alloy composition, Appl. Surf. Sci. 388 (2016) 294–303. https://doi.org/10.1016/j.apsusc.2016.01.046.

[45] C.L.A. Leung, S. Marussi, M. Towrie, R.C. Atwood, P.J. Withers, P.D. Lee, The effect of powder oxidation on defect formation in laser additive manufacturing, Acta Mater. 166 (2019) 294–305. https://doi.org/10.1016/j.actamat.2018.12.027.

[46] A. Raza, H. Jin, S. Hyung, Strength enhancement and density reduction by the addition of Al in CrFeMoV based high-entropy alloy fabricated through powder metallurgy, Mater. Des. 157 (2018) 97–104. https://doi.org/10.1016/j.matdes.2018.07.023.

[47] E. Hryha, C. Gierl, L. Nyborg, H. Danninger, E. Dudrova, Surface composition of the steel powders pre-alloyed with manganese, Appl. Surf. Sci. 256 (2010) 3946–3961. https://doi.org/10.1016/j.apsusc.2010.01.055.

[48] E. Hryha, E. Dudrova, L. Nyborg, On-line control of processing atmospheres for proper sintering of oxidation-sensitive PM steels, J. Mater. Process. Technol. 212 (2012) 977–987. https://doi.org/10.1016/j.jmatprotec.2011.12.008.

[49] C. Pauzon, A. Markström, S.D. Goff, E. Hryha, Effect of the Process Atmosphere Composition on Alloy 718 Produced by Laser Powder Bed Fusion, (2021).

[50] O.A. Quintana, J. Alvarez, R. Mcmillan, W. Tong, C. Tomonto, Effects of Reusing Ti-6Al-4V Powder in a Selective Laser Melting Additive System Operated in an Industrial Setting, Jom. 70 (2018) 1863–1869. https://doi.org/10.1007/s11837-018-3011-0.

[51] C. Pauzon, B. Hoppe, T. Pichler, S. Dubiez-Le Goff, P. Forêt, T. Nguyen, E. Hryha, Reduction of incandescent spatter with helium addition to the process gas during laser powder bed fusion of Ti-6Al-4V, CIRP J. Manuf. Sci. Technol. 35 (2021) 371–378. https://doi.org/10.1016/j.cirpj.2021.07.004.

[52] Z.A. Young, Q. Guo, N.D. Parab, C. Zhao, M. Qu, L.I. Escano, K. Fezzaa, W. Everhart, T. Sun, L. Chen, Types of spatter and their features and formation mechanisms in laser powder bed fusion additive manufacturing process, Addit. Manuf. 36 (2020) 101438. https://doi.org/10.1016/j.addma.2020.101438.

[53] Y. Liu, Y. Yang, S. Mai, D. Wang, C. Song, Investigation into spatter behavior during selective laser melting of AISI 316L stainless steel powder, Mater. Des. 87 (2015) 797–806. https://doi.org/10.1016/j.matdes.2015.08.086.

[54] S.A. Khairallah, A.T. Anderson, A. Rubenchik, W.E. King, Laser powder-bed fusion additive manufacturing: Physics of complex melt flow and formation mechanisms of pores, spatter, and denudation zones, Acta Mater. 108 (2016) 36–45. https://doi.org/10.1016/j.actamat.2016.02.014.

[55] S. Ly, A.M. Rubenchik, S.A. Khairallah, G. Guss, M.J. Matthews, Metal vapor micro-jet controls material redistribution in laser powder bed fusion additive manufacturing, Sci. Rep. 7 (2017) 1–12. https://doi.org/10.1038/s41598-017-04237-z.

[56] P. Moghimian, T. Poirié, M. Habibnejad-Korayem, J.A. Zavala, J. Kroeger, F. Marion, F. Larouche, Metal powders in additive manufacturing: A review on reusability and recyclability of common titanium, nickel and aluminum alloys, Addit. Manuf. 43 (2021). https://doi.org/10.1016/j.addma.2021.102017.

[57] L.E.L. PEEYUSH NANDWANA, WILLIAM H. PETER, RYAN R. DEHOFF, and S.S.B. MICHAEL M. KIRKA, FRANCISCO MEDINA, Recyclability Study on Inconel 718 and Ti-6Al-4V Powders for Use in Electron Beam Melting, Metall. Mater. Trans. B. 47 (2016) 754–762. https://doi.org/10.1007/s10884-015-9497-z.

[58] S. Ghods, E. Schultz, C. Wisdom, R. Schur, R. Pahuja, A. Montelione, D. Arola, M. Ramulu, Electron beam additive manufacturing of Ti6Al4V: Evolution of powder morphology and part microstructure with powder reuse, Materialia. 9 (2020) 100631. https://doi.org/10.1016/j.mtla.2020.100631.

[59] G. Shanbhag, M. Vlasea, The effect of reuse cycles on Ti-6Al-4V powder properties processed by electron beam powder bed fusion, Manuf. Lett. 25 (2020) 60–63. https://doi.org/10.1016/j.mfglet.2020.07.007.

[60] Y. Sun, M. Aindow, R.J. Hebert, The effect of recycling on the oxygen distribution in Ti-6Al-4V powder for additive manufacturing, Mater. High Temp. 35 (2018) 217–224. https://doi.org/10.1080/09603409.2017.1389133.

[61] V. Juechter, T. Scharowsky, R.F. Singer, C. Körner, Processing window and evaporation phenomena for Ti-6Al-4V produced by selective electron beam melting, Acta Mater. 76 (2014) 252–258. https://doi.org/10.1016/j.actamat.2014.05.037.

[62] D. Cormier, O. Harrysson, T. Mahale, H. West, Freeform Fabrication of Titanium Aluminide via Electron Beam Melting Using Prealloyed and Blended Powders, Res. Lett. Mater. Sci. 2007 (2007) 1–4. https://doi.org/10.1155/2007/34737.

[63] V. Petrovic, R. Niñerola, Powder recyclability in electron beam melting for aeronautical use, Aircr. Eng. Aerosp. Technol. 87 (2015) 147–155. https://doi.org/10.1108/AEAT-11-2013-0212.

[64] J. Schwerdtfeger, C. Körner, Selective electron beam melting of Ti-48Al-2Nb-2Cr: Microstructure and aluminium loss, Intermetallics. 49 (2014) 29–35. https://doi.org/10.1016/j.intermet.2014.01.004.

[65] E. Damri, E. Tiferet, D. Braun, Y.I. Ganor, M. Chonin, I. Orion, Effects of gas pressure during electron beam energy deposition in the ebm additive manufacturing process, Metals (Basel). 11 (2021) 1–13. https://doi.org/10.3390/met11040601.

[66] T. Fiegl, M. Franke, C. Körner, Impact of build envelope on the properties of additive manufactured parts from AlSi10Mg, Opt. Laser Technol. 111 (2019) 51–57. https://doi.org/10.1016/j.optlastec.2018.08.050.

[67] M.C. Chaturvedi, Y.F. Han, Strengthening mechanisms in Inconel 718 superalloy, Met. Sci. 17 (1983) 1–5. https://doi.org/10.1179/030634583790421032.

[68] E.A. Loria, The Status and Prospects of Alloy 718, Jom. 40 (1988) 36–41. https://doi.org/10.1007/BF03258149.

[69] N. Brodusch, H. Demers, R. Gauvin, Field Emission Scanning Electron Microscopy. [electronic resource] : New Perspectives for Materials Characterization., 2018. https://search.ebscohost.com/login.aspx?direct=true&AuthType=sso&db=cat07472a&AN=clec.SPRINGERLINK9789811044335&site=eds-live&scope=site&custid=s3911979&authtype=sso&group=main&profile=eds%0Ahttps://cthliblicenses.azurewebsites.net/License?id=354%0Ahttp:/.

[70] A. Ul-Hamid, A Beginners' Guide to Scanning Electron Microscopy, 2018. https://doi.org/10.1007/978-3-319-98482-7.

[71] C. Oikonomou, E. Hryha, L. Nyborg, Development of methodology for surface analysis of soft magnetic composite powders, Surf. Interface Anal. 44 (2012) 1166–1170. https://doi.org/10.1002/sia.3848.

[72] B.A. Taleatu, E. Omotoso, C. Lal, W.O. Makinde, K.T. Ogundele, E. Ajenifuja, A.R. Lasisi, M.A. Eleruja, G.T. Mola, XPS and some surface characterizations of electrodeposited MgO nanostructure, Surf. Interface Anal. 46 (2014) 372–377. https://doi.org/10.1002/sia.5425.

[73] J.F. Moulder, W.F. Stickle, P.E. Sobol, K.D. Bomben, Handbook of X-ray photoelectron spectroscopy: a reference book of standard spectra for identification and interpretation of XPS data; Physical Electronics: Eden Prairie, MN, 1995, (2000) 261. https://www.cnyn.unam.mx/~wencel/XPS/MANXPS.pdf.